AFOSR-TR- 79-0022

BOUNDARY LAYER SEPARATION FROM A SLENDER BODY AT HIGH ANGLES OF ATTACK

by

C. E. G. Przirembel
D. T. G. Wen

Final Report
October 1978

Prepared Under Grant No. AFOSR-77-3300
for the
Department of the Air Force
Air Force Office of Scientific Research
Bolling Air Force Base, D.C. 20332

RU-TR 151-MIAE-F

Department of
Mechanical, Industrial and Aerospace Engineering
College of Engineering

RUTGERS
THE STATE UNIVERSITY OF NEW JERSEY

New Brunswick, New Jersey 08903

AIR FORCE OFFICE OF SCIENTIFIC RESEARCH (AFSC)
NOTICE OF TRANSMITTAL TO DDC
This technical report has been reviewed and is
approved for public release IAW AFR 190-12 (7b).
Distribution is unlimited.
A. D. BLOSE
Technical Information Officer

RU-TR 151-MIAE-F

BOUNDARY LAYER SEPARATION FROM A SLENDER BODY AT HIGH ANGLES OF ATTACK

Final Technical Report

for

1 March 1977 to 30 June 1978

C. E. G. Przirembel
and
D. T. G. Wen

October 1978

Submitted to:

Department of the Air Force
Air Force Office of Scientific Research
Bolling Air Force Base, D.C. 20332

Prepared by:

Department of Mechanical, Industrial & Aerospace Engineering
Rutgers University - The State University of New Jersey
New Brunswick, New Jersey

FOREWORD

This report has been prepared by the Department of Mechanical, Industrial, and Aerospace Engineering, Rutgers University, New Brunswick, New Jersey, under Grant No. AFOSR-77-3300 and covers the period 1 March 1977 - 30 June 1978.

The work reported herein was performed for the Department of the Air Force, Air Force Office of Scientific Research, Bolling Air Force Base, D.C. 20332. The technical direction was provided by Lieutenant Colonel Robert C. Smith of AFOSR/NA.

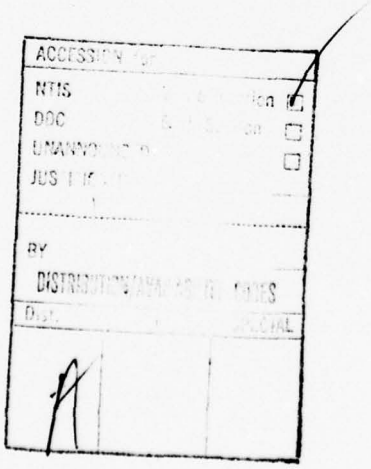

ABSTRACT

The boundary layer separation process associated with the flow field around a slender body of revolution at moderate to high angles of attack was investigated. Based on extensive comparisons with existing, two-dimensional turbulent separation data, flow separation criteria by Stratford, and Sandborn and Liu were selected for the slender body calculations. The two primary, axial separation lines were obtained by applying the separation criteria to the measured, surface pressure distributions in numerous crossflow planes. The location of the origin of the asymmetric vortices were predicted by applying Stratford's separation criterion to the pressure distribution along the previously calculated axial separation lines. Good agreement between the analytical and experimental points was obtained. Correlation between the side force maxima or minima and the location of the origin of the asymmetric vortices was inconclusive. The need for more detailed experimental data is discussed.

TABLE OF CONTENTS

LIST OF FIGURES

NOMENCLATURE

X - distance from the actual leading edge

x - distance from the equivalent leading edge

U,V - velocity

C_p - pressure coefficient

C_f - local skin friction coefficient

C_d - drag coefficient

Re - Reynolds number

ν - kinematic viscosity

$\frac{d}{h}$ - blockage ratio (see reference 14)

H - shape factor

δ^* - displacement thickness

δ - boundary layer thickness

C - constant

θ - angular location measured from stagnation point

α - angle of attack

ϕ - roll angle

M - Mach number

R - radius of model

D - diameter of model

Subscripts

o - start of adverse pressure gradient

∞ - free stream condition

t - transition

$s.$ - separation

$p.s.$ - pre-separation

prime - measured quantity which has not been corrected for blockage effect (see reference 14)

1.0 INTRODUCTION

Slender bodies of revolution moving at high angles of attack at subsonic/supersonic speed are known to experience large side forces and yawing moments (1). These forces and yawing moments have been of major concern in the design of modern aircrafts. Especially in recent years, with the advent of missiles and supersonic aircrafts, where the body is a major contributor to the aerodynamic behavior of the system, a thorough understanding of this aerodynamic problem has become more and more critical.

When a supersonic aircraft with a pointed fuselage forebody is flying at extremely high angles of attack, such as those occuring during post-stall flights and spins, large asymmetric yawing moments may be produced by the vehicle geometry. These moments can be significantly larger than the moments generated by the deflection of conventional control surfaces. As a result instabilities and control difficulties may be experienced by the aircraft. As a matter of fact, some recent losses of modern aircrafts are attributed to this problem. As to missiles, one of the possibilities of launching the MX missile is to use a transport aircraft. During the launching stage, the missile is exposed to high subsonic/transonic flow at high angles of attack and at high free stream Reynolds numbers. The same flight environment also exists during the launching of air to air missiles from strategic aircrafts. Although in both cases this unfavorable situation exists for only a very short period of time, the determination and control of the side forces and moments is crucial to the completion of the desired mission.

In viewing the overall fluid dynamic problem of the flow about bodies of revolution, it is essential to fully understand the various flow patterns associated with the entire spectrum of angles of attack. It is now well-established that a slender body of revolution moving in a real fluid field may develop several distinct flow patterns, depending upon its angle of attack. For angles of attack from 0 to 5 degrees, the flow does not separate and can be described by a potential flow field and an attached laminar or turbulent boundary layer. For angles of attack between 5 and 25 degrees, flow separation occurs. A steady symmetric vortex pair is shed, as shown in Figure 1. No side forces are generated because of the symmetry of the flow. At angles of attack between 25 and 50 degrees, the symmetric vortex cores become asymmetric and break away from the body from alternate sides, as shown in Figure 2. This steady asymmetric flow field produces considerable side forces. As the angle of attack increases to between 50 and 75 degrees, the steady asymmetric flow field becomes unsteady and alternates back and forth. Finally, for angles of attack above 70 degrees, the flow pattern degenerates into a classical wake normally associated with right circular cylinders. The current study is primarily focussed on the range of 25 to 50 degrees of angles of attack where the vortex shedding is steady and asymmetric, and large side forces exist.

In addition to the angle of attack, there are many other factors that affect the flow. These include Mach number, Reynolds number, nose fineness ratio, and nose bluntness (1). It has also been shown by many investigators that roll angle and/or nose misalignment play a very important role in the variation of side forces and yawing moments. This implies that unless a

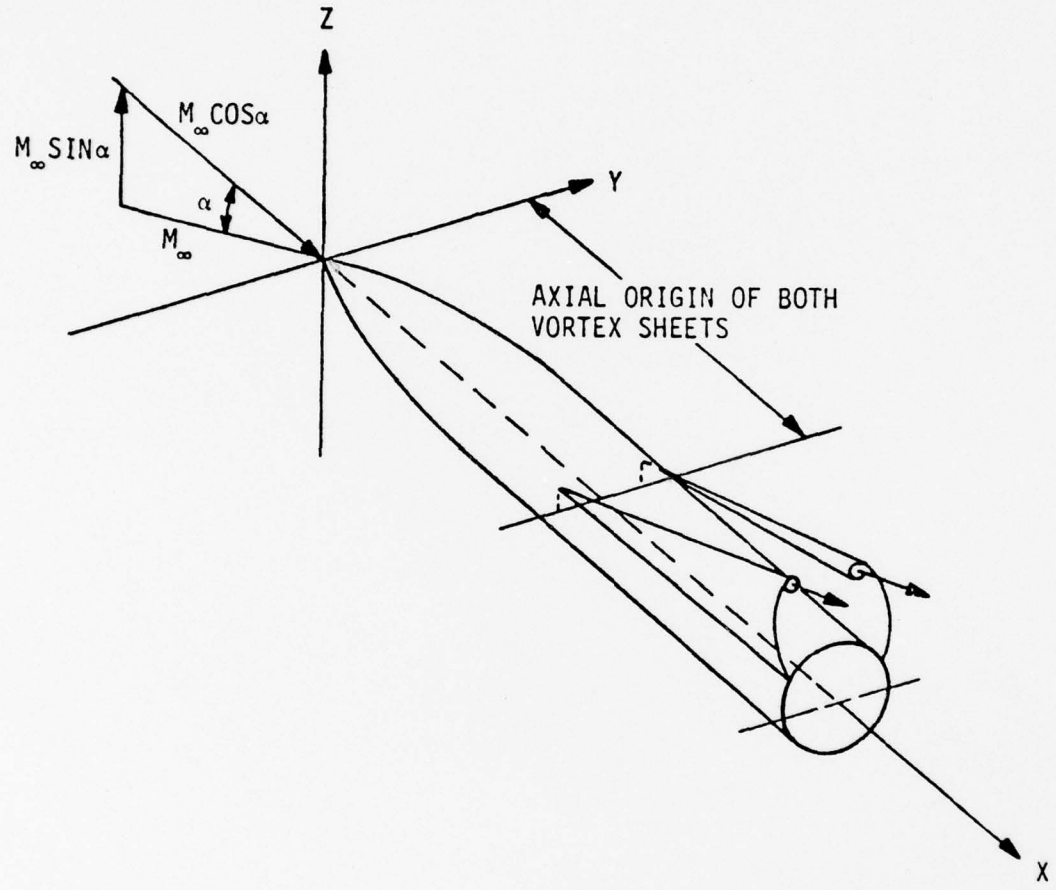

FIGURE 1 STEADY, SYMMETRIC VORTEX SHEDDING FOR ANGLES OF ATTACK BETWEEN 5 AND 25 DEG.

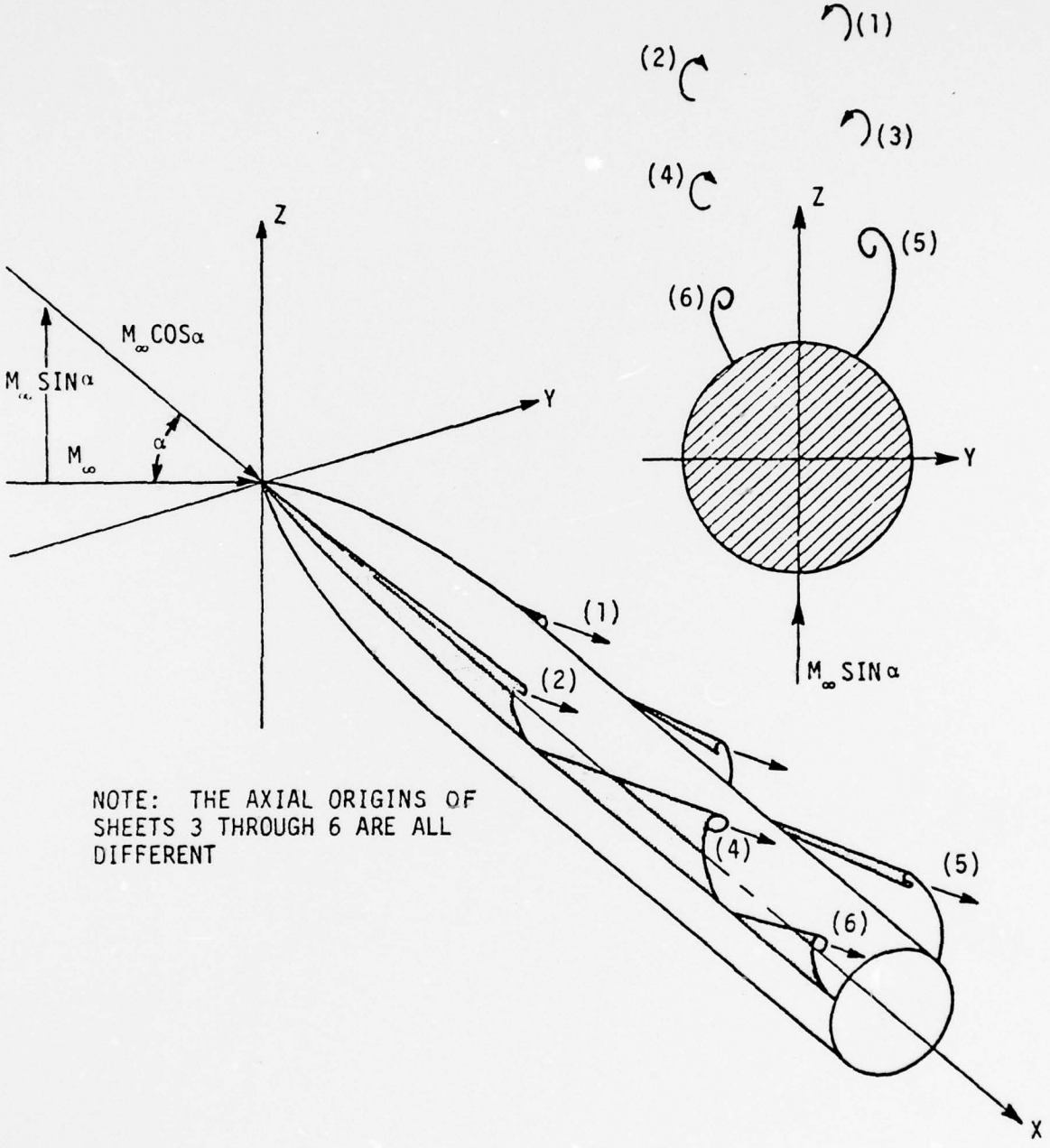

NOTE: THE AXIAL ORIGINS OF SHEETS 3 THROUGH 6 ARE ALL DIFFERENT

FIGURE 2 ASYMMETRIC VORTEX SHEDDING FOR ANGLES OF ATTACK BETWEEN 25 AND 50 DEG.

particular model has been tested at several roll angles, the selected data may not represent the maximum side forces or yawing moments. From numerous wind tunnel investigations, researchers have generally agreed that increasing Mach number, decreasing nose fineness ratio, and a slight nose bluntness reduce side forces. Nevertheless, existing experimental data have shown conflicting and often confusing results on the effect of Reynolds number. For example, Fleeman and Nelson (2) showed significant variation of both the side force and yawing moment with Reynolds number. For a model with a tangent ogive nose and a cylindrical afterbody, the side force and yawing moment increase up to free stream Reynolds number of 2.5×10^5, and then decrease with increasing Reynolds number. Peak values of the side force and yawing moment occurred at cross flow Reynolds numbers between 1.4×10^5 and 2.5×10^5. However, for approximately the same free stream Reynolds number, Coe, Chamber, and Letko (3) observed no significant variation of side forces and yawing moments. Hence, more work needs to be done to establish the Reynolds number dependency of these large side forces and yawing moments.

As mentioned earlier, for large angles of attack the flow on the lee side of an axisymmetric body separates and rolls up into regions of concentrated vorticity. To predict the order of magnitude of the resulting side forces and yawing moments, Deffenbaugh and Koerner (4) extended the method of calculating the flow about a body of revolution for moderate cross flow Reynolds numbers, $Re < 10^5$, at angles of attack less than 25 degrees to high cross Reynolds numbers, $10^6 < Re < 10^7$, by using Stratford's separation criterion (9) to determine the separation of the turbulent boundary layer on the cylindrical portion of the model. The necessary pressure distribution was obtained from the inviscid outer flow calculation.

The viscous flow on the nose of the missile was calculated by solving the unsteady laminar boundary layer finite difference equations. The results gave good agreement with experimental data for the normal force coefficient and pitching moment coefficient for sharp-nosed missile models. However, the side force variation was consistantly underestimated.

In addition to developing some understanding of the boundary layer separation and vortex shedding problems, it was the objective of the current study to analyze some carefully selected surface pressure data, which have been obtained in an on-going, multi-phase, wind tunnel test program designed to investigate the aerodynamics of advanced missiles. Since no flow visualization data were available for these models, a suitable, turbulent separation point prediction technique was selected and applied to the surface pressure data in the cross-flow planes. The resulting axial distribution of the two primary separation lines were then investigated by comparing them with the calculated axial distribution of the side force. Of particular interest was any characteristic angular location change in the separation line at the axial location of side force maxima and minima.

Three two-dimensional, turbulent separation criteria, which are currently available in the literature, were investigated; and one separation criterion was selected. The description of each criterion is given in the following section.

2.0 LITERATURE REVIEW

Flow separation occurs when the pressure increase in the streamwise direction becomes so large that the momentum associated with the fluid near the wall is just balanced. In the design of airfoils, it is necessary to avoid flow separation in order to keep drag levels low. Especially in designing for high-lift, predicting separation points is a crucial part of the design problem. Many methods have been derived to determine the location of separation based on the fact that the time-averaged, two-dimensional flow separation is characterized by zero skin friction. Among flow separation problems, steady two-dimensional laminar flow separation is the most fundamental. For laminar separation, high accuracy can be obtained by using current prediction methods. For turbulent flows, however, because of the lack of thorough understanding of the mechanics of turbulence, empirical investigations are needed to justify the analytical predictions. Thus, the predictions of separation in turbulent flows using currently prevailing methods must be checked against experiments. The current prediction methods on separation in turbulent flow can be divided into two groups. The first group requires the detailed solution of the boundary layer equations. Methods in this group require the solution of either partial differential equations or momentum integral equations. For two-dimensional and axisymmetric incompressible flow, Cebeci and Smith's method (5) is an example of the differential method, and Truckenbrodt's method (6) is an example of energy integral method, and Head's method (7) is a momentum integral method. In solving the governing intergral equations, the parameter used to predict the separation is zero wall shear stress, where-

as, in the integral methods the shape factor $H = \delta^*/\theta$ is used to locate the separation. Separation occurs as H reaches a value between 1.8 and 2.4 (8). The second group of prediction methods does not require tedious calculations of boundary layer equations, but they use the composite nature of the turbulent boundary layer. Separation is located by simple differential equations together with some experimentally determined factors or constants. For example, Stratford (9) divides the turbulent boundary layer into inner and outer layers. His analysis is based on two assumptions, namely (1) in the inner layer, the adverse pressure is balanced by the shear force, and (2) in the outer layer, the adverse pressure only causes a general lowering of the dynamic head. Following the same concepts of treating the boundary layer as inner and outer regions but with different mathematical approaches, Townsend (10) and Sandborn and Liu (11), derived their prediction methods. These three methods are discussed in detail in the next sections.

2.1 Stratford's Criteria (9)

Stratford's method (9) is based on the postulation that the turbulent boundary layer in a pressure rise could be divided into two distinct regions, the inner layer and the outer layer. In the outer layer it is assumed that the effect of pressure rise will only cause general lowering of the velocity profile, i.e., the shear forces are small compared with either inertia forces or the pressure gradient. Therefore, the back pressure force is balanced by the fluid inertia force. In the inner layer, due to the fact that inertia forces at the wall are zero, the pressure forces are primarily balanced by the gradient of the shear force. Joining the

two layers and assuming that the skin friction is zero when the flow reaches the separation condition, Stratford established his separation criterion as follows:

$$C_p\left[x\,\frac{dC_p}{dx}\right]^{1/2}(10^{-6}\,Re)^{-0.1} = C \qquad (1)$$

This criterion is valid for an adverse pressure gradient following the point where the pressure is minimum, as shown in Figure 3. The pressure coefficient, C_p, is based on the conditions at the point of minimum pressure. The distance x is measured from a ficticious stagnation point corresponding to an upstream condition of flow over a flat plate with zero pressure gradient. If the upstream laminar region is very short and an instantaneous transition is assumed then X_o, the distance between the ficticious stagnation point and the point of minimum pressure, can be calculated by the following equation:

$$X_o = \int_o^{X_o}\left(\frac{U}{U_o}\right)^3 dx \qquad (2)$$

where X is the distance from the actual leading edge. In order to compensate for the laminar and transition region, the following equation is used:

$$X_o = 38.2\left(\frac{\nu}{x_t u_t}\right)^{3/8}\left(\frac{U_o}{U_t}\right)^{1/8}\left[\int_o^{X_t}\left(\frac{U}{U_o}\right)^5 d\left(\frac{x}{x_t}\right)\right]^{5/8} x_t + \int_{x_t}^{x_o}\left(\frac{U}{U_o}\right)^3 dx \qquad (3)$$

The Reynolds number is based on the properties at the point of minimum pressure and the equivalent distance. C is a constant which is determined from the concept of a mixing length in conjunction with experiments. For C greater than 0.4, separation is predicted when C = 0.4. If C lies be-

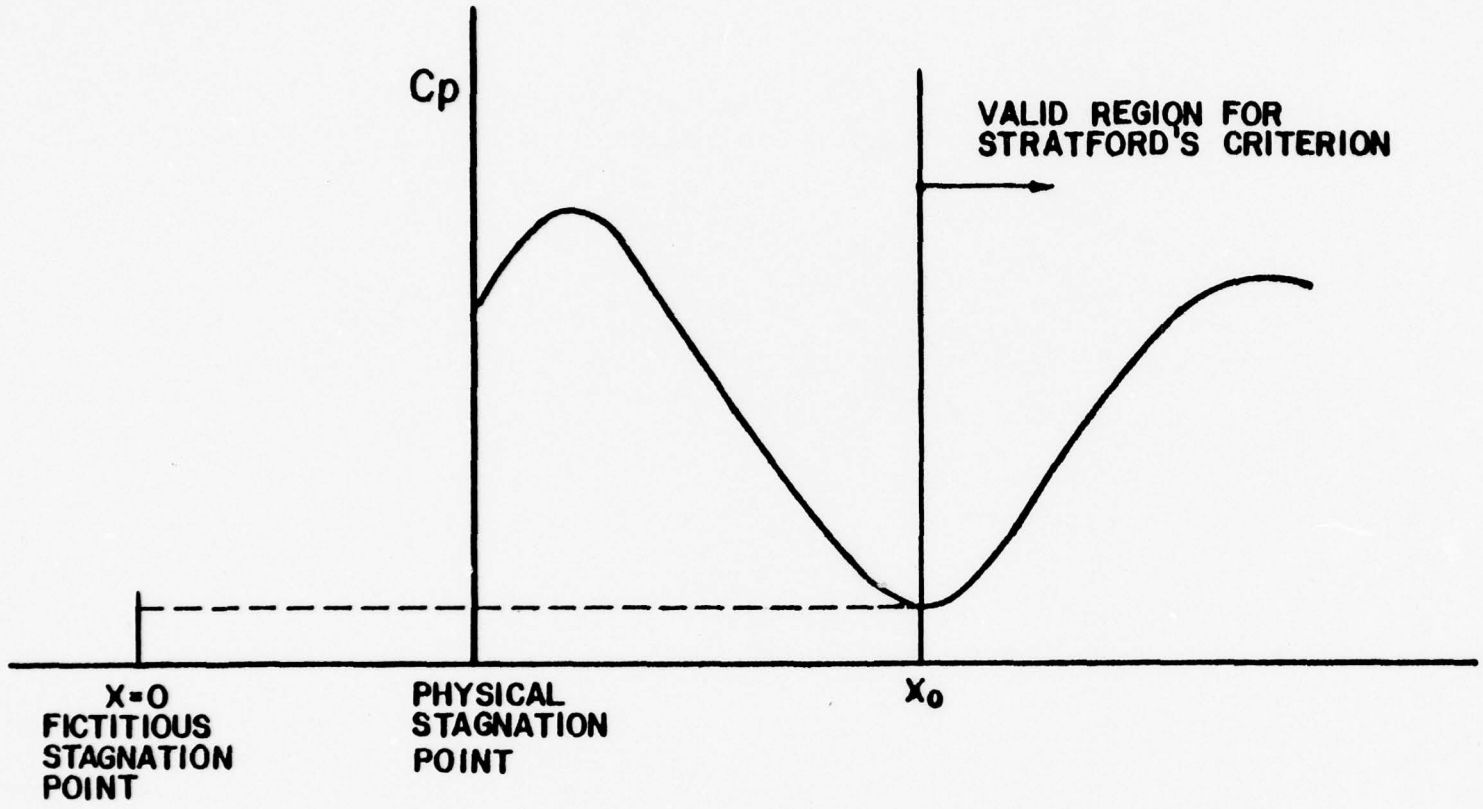

FIGURE 3 VALID REGION OF PRESSURE GRADIENT
—STRATFORD'S CRITERION

tween 0.35 and 0.4, separation occurs at the maximum value of C. If C is less than 0.35, no separation would occur.

2.2 Townsend's Criterion (10)

Townsend followed Stratford's general ideas and derived a more comprehensive theory. His criterion was given in the expression:

$$\mathrm{Log}\left(\frac{U_o}{\nu}\right)\left(\frac{dx}{dCp}\right)_{ps} C_{fo}^{1.5} = \left(\frac{1}{2.98}\frac{C_p}{C_{fo}} + 2.7\right)^{1/2} + \mathrm{Log}\left[\left(\frac{1}{2.98}\frac{C_p}{C_{fo}} + 2.7\right)^{1/2} - 1\right] - C \qquad (4)$$

In the equation, $\left(\frac{dC_p}{dx}\right)_{ps}$ is the pressure gradient prior to the separation point; C_{fo} is the skin friction at the point where the adverse pressure starts growing, and C is a constant, which, Townsend suggested from experiments, to have the value of 3.472. Townsend's criterion is sometimes difficult to apply, for it is often very difficult to determine the pressure gradient upstream of separation, namely, $\left(\frac{dC_p}{dx}\right)_{ps}$. Also, Townsend's criterion is a strong function of the skin friction at the point of minimum pressure, C_{fo}. Furthermore, Townsend's criterion predicts only the separation pressure, not the separation point location.

2.3 Sandborn and Liu's Criterion (11)

Following an analytic approach similar to Stratford, Sandborn and Liu derived their prediction criterion which has the form:

$$C_p^{1/4(2n-1)}\left(X_s\frac{dCp}{dx}\right)^{1/2} \simeq 0.22\ C \qquad (5)$$

In the expression, n is an integer from the power law of the velocity profile; C is a constant which has the value of 0.377 for n = 6 and 0.24 for n = 8. The selection of n is that the highest value of n will give the

highest possible separation pressure.

In his research, Sandborn recognized an intermittent separation region before the steady separation occurs. In this region, intermittent streaks of back flow were observed which most experimenters identified as turbulent separation. To incorporate both the intermittent and fully developed turbulent separated flow regions, Sandborn postulated that: (1) the intermittent separation velocity profile, which still has a finite value at the surface, would be equivalent to an adverse pressure gradient in the laminar boundary layer, and (2) the fully turbulent separation profile would be equivalent to a laminar separation profile. Through empirical means, the velocity distribution for intermittent separation was correlated with the form factor, H, where $H = 1 + (1 - \frac{\delta^*}{\delta})^{-1}$. The minimum value of H for intermittent separation is 2. With these assumptions, the boundary layer equations can be solved. In solving the boundary layer equations, instead of using mixing length theory as in Stratford's criterion, an eddy viscosity theory was used. Combining the solution of the boundary layer equations and an upstream power law velocity profile, the location of separation, x_s, is obtained from the relation as shown in the beginning of this section. Constants in the formula were estimated experimentally. It is worthwhile to note that Sandborn and Liu's criterion is independent of the Reynolds number.

3.0 APPRAISAL OF SEPARATION CRITERIA

Five experimentally determined separated flows were used to evaluate the applicability of Stratford's and Sandborn and Liu's criteria for the prediction of separation in turbulent flows. Because of the lack of tabulated data in some of the reported results, the necessary pressure data were acquired from the pressure distribution curves. This procedure had some detrimental effect on the overall accuracy of the calculation. However, the primary purpose of using these experimental data was only to establish the general validity of these two criteria.

3.1 Schubauer's Air Foil (12)

This experiment was carried out in an open-air wind tunnel with a 10 feet (3.05 m) high test section at the National Bureau of Standards. The test model was a 10 feet (3.05 m) high, and 27.9 feet (8.5 m) long, air-foil-like wall, constructed of 1/4 inch (6.35mm) transite on a wooden frame, and finished and polished on the working side. A schematic drawing of the model is shown in Figure 4. During the test, the actual flow conditions were incompressible, two-dimensional, and with 0.5% turbulence in the free stream. All the measurements were taken with a static pressure tube 0.004 inch (0.1 mm) in diameter at free stream velocity of about 160 fps (48.77 m/s) at the 17-1/2 (5.33 m) position. The static pressure distribution is shown in Figure 5. The boundary layer thickness at 17-1/2 feet (5.33 m) on the model was equivalent to that on a flat plate 14.3 feet long (4.36 m) with a fully turbulent boundary layer and a zero pressure gradient. The Reynolds number for a flat plate corresponding to 160 fps (48.77 m/s) is 14.3×10^6. Separation was located at 25.7 $\pm$ 0.2 feet

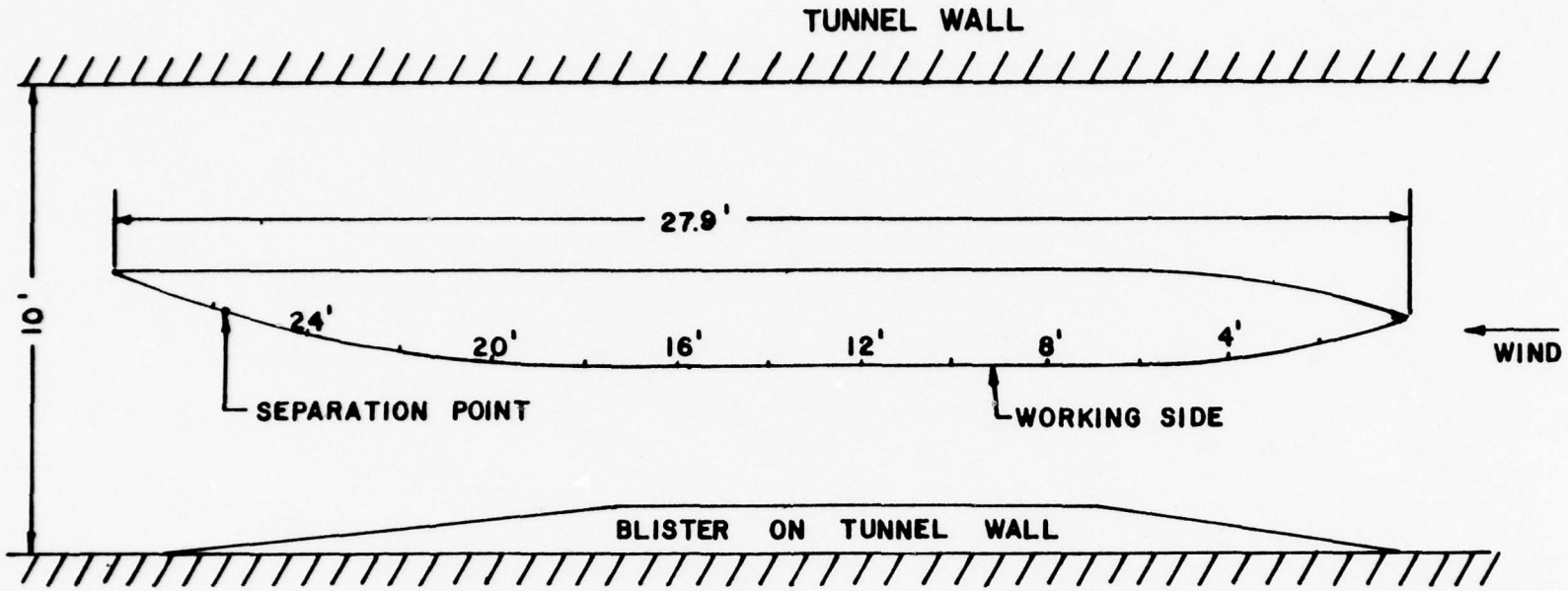

FIGURE 4 SKETCH OF AIR FOIL MODEL

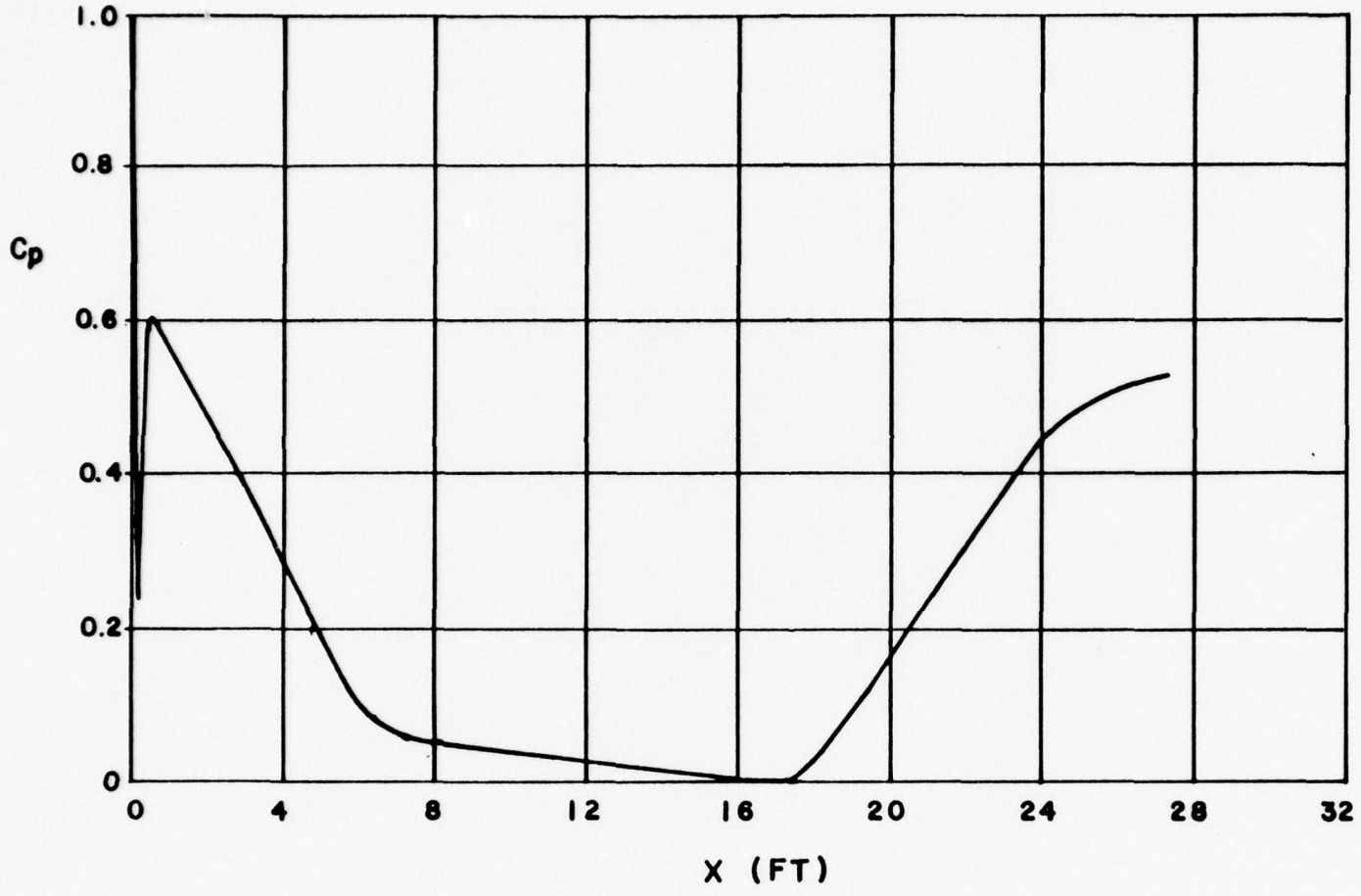

FIGURE 5 PRESSURE DISTRIBUTION CURVE FOR THE AIR FOIL MODEL

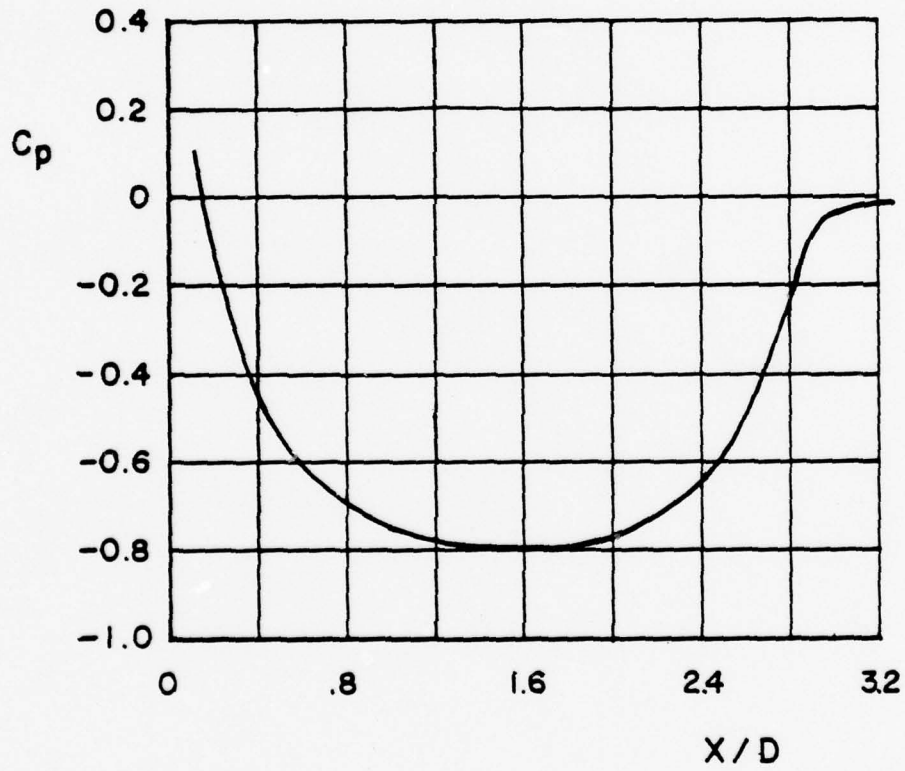

FIGURE 6 PRESSURE DISTRIBUTION CURVE FOR THE ELLIPTIC CYLINDER MODEL

(7.83 $\pm$ 0.061 m) in the experiment.

3.2 Schubauer's Elliptic Cylinder (13)

In this experiment, Schubauer investigated flow separation over an elliptic cylinder 4-1/2 feet (1.37 m) long with major axis 11.78 in (299 mm) and minor axis 3.98 in (101 mm). Measurements were taken with 21 orifices located 2-1/2 feet below center of the model. Eighteen of the orifices were around the side to measure static pressures in the boundary layer, one at the leading edge, and two on the opposite side near the leading edge to align the model with its major axis parallel to the free stream. A one inch mesh wire screen was placed at 18 inches (457 mm) ahead of the leading edge of the model to increase the turbulence in the flow. The free stream velocity was 16 ft/sec (4.88 m/sec). The Reynolds number based on the free stream velocity and the minor axis of the model was 1.18×10^5. Separation was observed at X/D = 2.91, where D is the length of the minor axis. Pressure data used in the current study was obtained from the pressure distribution curve as shown in Figure 10 in Schubauer's paper. A copy of this curve is in Figure 6.

3.3 Roshko's Circular Cylinder (14)

Roshko's experiment was conducted in the Southern California Co-operative Wind Tunnel, which was disassembled after the experiment. This tunnel had a test section of 8-1/2 feet (2.59 m) high and 11 ft (3.35 m) wide. In the experiment, the flow speed was limited to about M = 0.25 in order to eliminate compressibility effects.

The model used in this experiment was made of a seamless black steel pipe, 18 inches (457 mm) in diameter. It was sandblasted to remove the protective paint and scale. The resulting surface roughness is 200 μ in (5.08×10^{-3} mm). The model was mounted in the center of the test section and spanned the entire 8-1/2 ft (2.59 m) height.

Pressure orifices were located every 10 degrees over half of the circumference. They were connected to a pressure measuring system. The sensitivity of the system was set to give full output at the highest dynamic pressure. Furthermore, a splitter plate was installed on the center line behind the cylinder. It also spanned the entire height of the test section and extended 4ft (1.22 m) along the center line. Corrections were made with the following equations to compensate for the wall interference upon the velocity and pressure coefficients:

$$\frac{V}{V'} = 1 + 1/4\, C_d' \left(\frac{d}{h} \right) + 0.82 \left(\frac{d}{h} \right)^2 \tag{6}$$

$$(C_p - 1) = \left(\frac{V'}{V} \right)^2 (C_p' - 1) \tag{7}$$

The Reynolds number was also corrected with the same equation as for velocity. A curve of corrected pressure coefficients, C_p, against θ, the angle measured from the stagnation point, at Reynolds number of 8.4×10^6 was shown in Figure 7. This curve was selected in the present research for verification of the separation criteria.

Roshko did not give the experimental separation point. Nevertheless, Cebeci (8) used the same set of data on separation prediction with various criteria, in which Stratford and Sandborn and Liu's methods were also

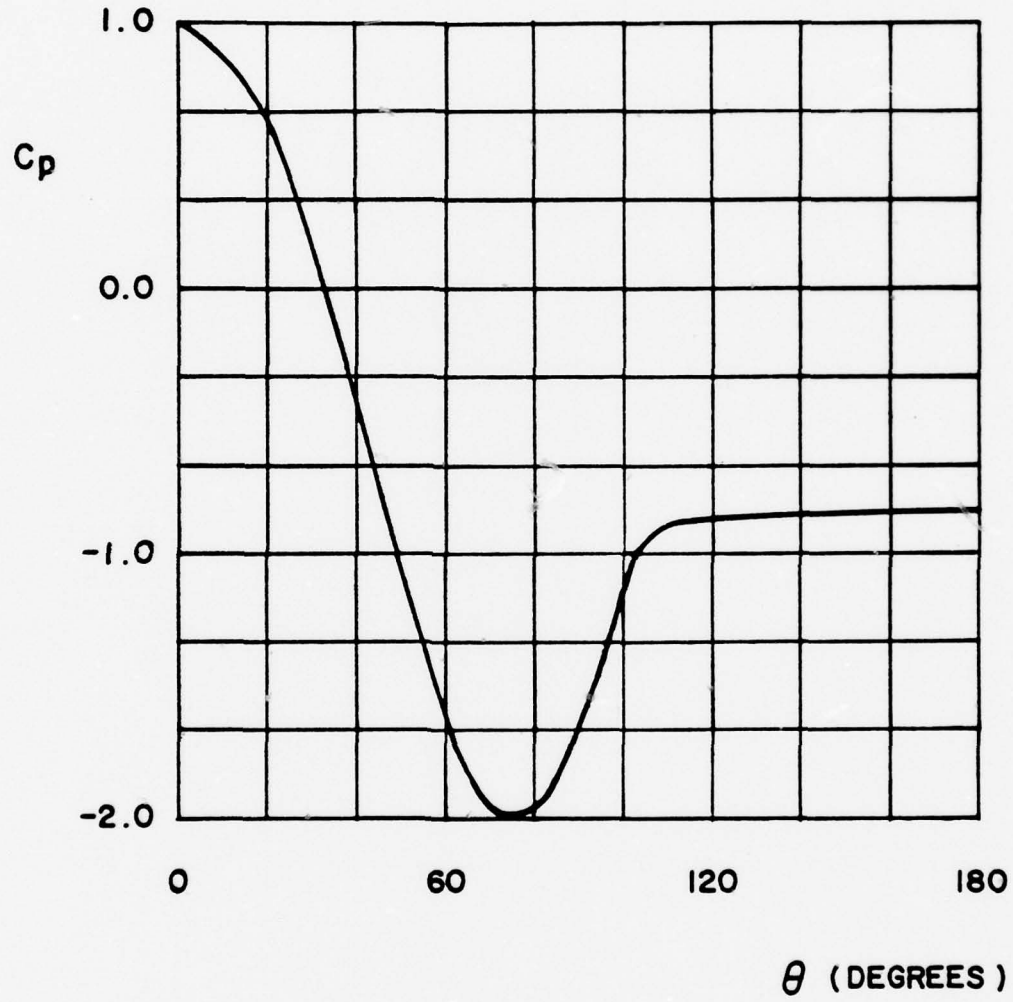

FIGURE 7 PRESSURE DISTRIBUTION CURVE FOR ROSHKO'S CIRCULAR CYLINDER

included. The results of Cebeci's calculation and the calculation in this paper are not exactly the same. The reason for the difference is assumed to be due to the inaccuracy introduced in the reading of the data from the curve. The results are shown in Section 3.6.

3.4 Yi's Elliptic Afterbody (15)

Yi's study was focussed on the separation of an incompressible turbulent boundary layer from an axisymmetric curved afterbody. The basic model was a circular cylinder with a diameter of 2-1/2 inches (63.5 mm). A semi-ellipsoidal base of axis ratio 4:1 was attached. In the experiment, the free stream velocity was kept at 155 ft/sec (47.2m/sec) with a corresponding unit Reynolds number of 0.939×10^6 per foot and Mach number of 0.136. A ring-shaped trip with a 1/2 inch (12.7 mm) high triangular cross-section was mounted at 10 radii upstream from the base of the model to insure a fully developed turbulent boundary layer in the test model. Measurements were made by pressure probes and hot wire probes. A graph of the static pressure distribution is shown in Figure 8. Separation was located by various techniques, such as oil film flow, "tell-tail" traverse, and smoke and water injection. Separation was located at 0.38 model radii upstream from the base.

3.5 Achenbach's Circular Cylinder (16)

This experiment was performed in a pressurized wind tunnel which had a rectangular test section of 19.7 in x 35.4 in (500 mm x 900 mm). The model was a brass tube, 5.9 in (150 mm) in diameter and 19.7 in (500 mm) in length. A schematic diagram is shown in Figure 9. Pressure

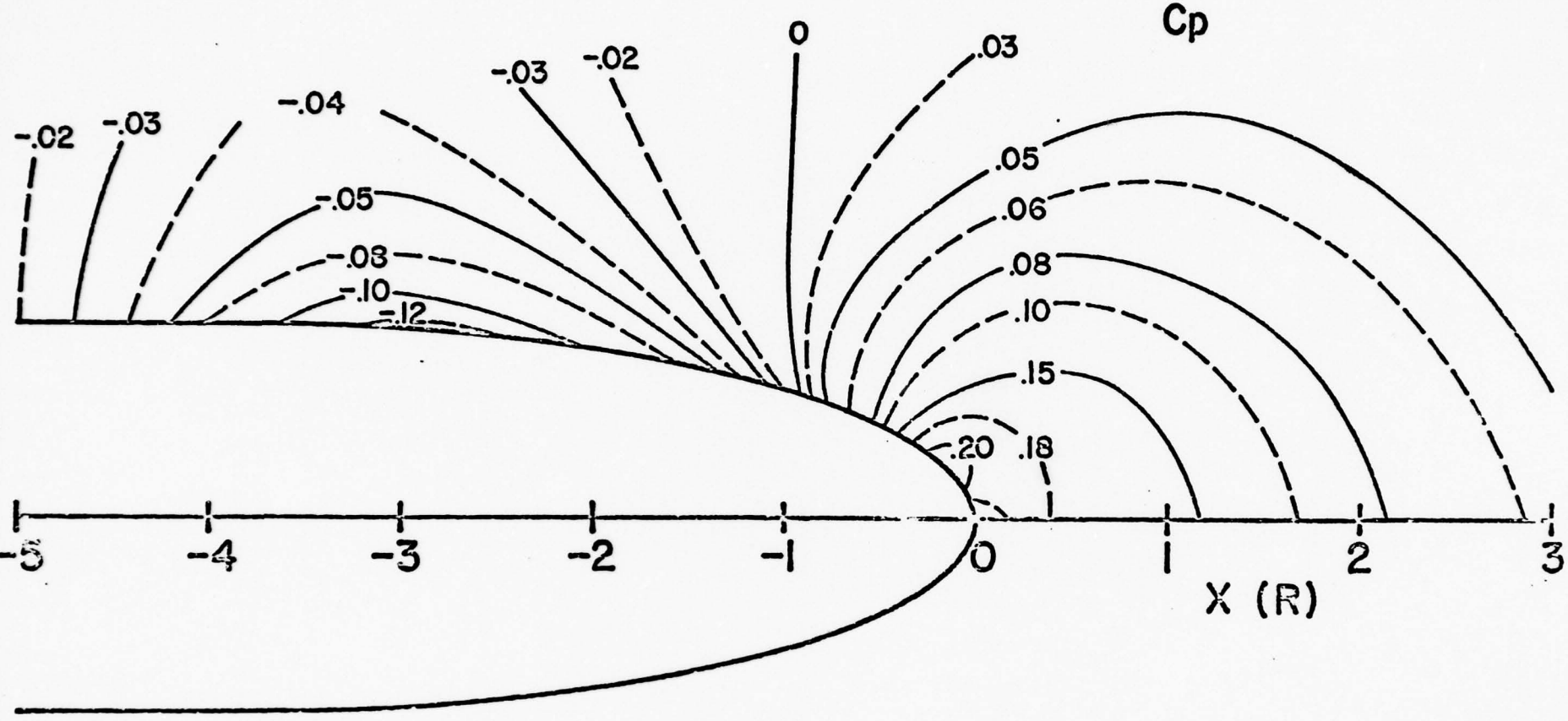

FIGURE 8 STATIC PRESSURE MAP OF YI'S MODEL

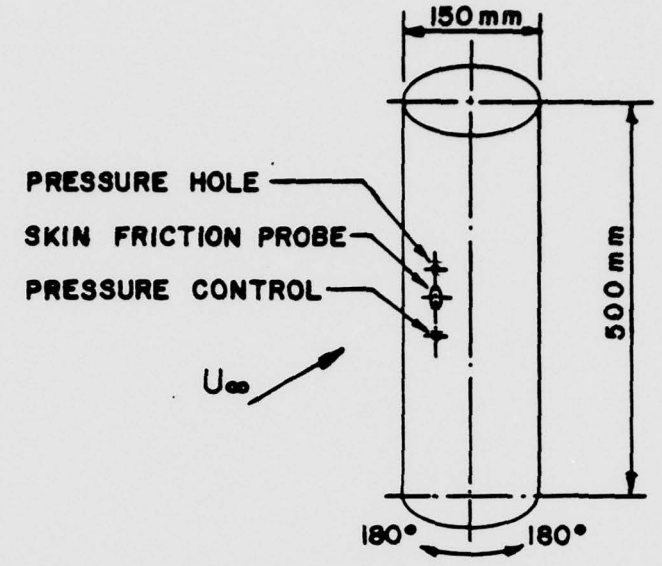

FIGURE 9 SKETCH OF ACHENBACH'S CIRCULAR CYLINDER

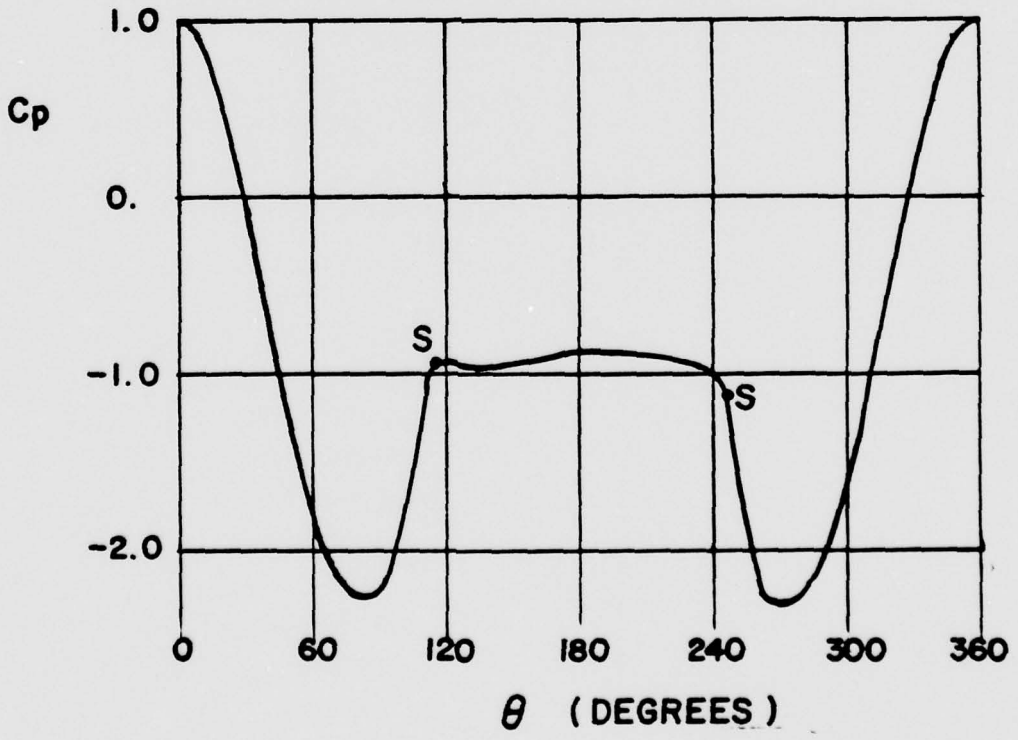

FIGURE 10 PRESSURE DISTRIBUTION CURVE FOR ACHENBACH'S CIRCULAR CYLINDER

data along the circumference were measured by rotating the cylinder at 5^{o} increments. A plot of pressure coefficient versus peripheral rotating angle, θ, is shown in Figure 10. The Reynolds number for this set of data was 3.6×10^{6}.

In this experiment, skin friction was also measured, and separation was determined by locating the point where the skin friction curve crossed the zero line. The results are in Section 3.6.

3.6 Results

For Schubauer's air foil model, the pressure data used in the computations were taken directly from Table I in the NACA report. The experimental separation point was found at X = 25.7 $\pm$ 0.2 ft (7.83 $\pm$ 0.061 m), where X was measured from the nose of the model along the model surface. With Stratford's criterion, the separation point was predicted at X = 24.2 ft (7.38 m) by interpolation. This gives an error of 5.8%. The same set of data was used by Stratford and the result was 24 ft (7.32 m). Using n = 6 and n = 8, the separation point was calculated at 25 ft (7.62 m), which represents a 2.7% error in Sandborn and Liu's criterion.

For Schubauer's elliptical cylinder, both methods give very close predictions. Stratford's method predicts the separation point at X/D = 2.89, 0.7% error; Sandborn and Liu's criterion predicts X/D = 2.89 for n = 6, and X/D = 2.95 for n = 8. These compare to the experimental result of X/D = 2.91. However, the results of the calculation are quite different from Cebeci's result (8) using Stratford's method. The reason, as indicated in the previous section, may be due to the inaccuracies in obtaining the data.

For Roshko's circular cylindrical model, Stratford's method did not predict separation. However, when the velocity distribution was extrapolated, separation was predicted at θ = 105 degrees. Cebeci observed the same problem, but then calculated separation at 120 degrees using Stratford's method. Sandborn and Liu's method predicted separation at θ = 105 degrees for both n = 6 and n = 8.

For Yi's elliptic afterbody model, Stratford's method predicted separation at X = -0.45R; Sandborn and Liu's method predicted separation at X = -0.447R for both n = 6 and n = 8. The negative sign means that X was measured in a direction opposite to the free stream. These compare to the experimental result of X = -0.38R. R is the radius of the cylindrical portion of the model.

Finally, for Achenbach's circular cylinder, the experimental separation point was found at 115 degrees. Stratford's method gave 105 degrees, 8.8% error. Sandborn and Liu's method gave 110 degrees, 4.6% error, for both n = 6 and n = 8.

From the above analysis, it was observed that both Stratford's, and Sandborn and Liu's criteria tend to predict the separation point earlier than the experimental results. The error is less than 10%. The results are summarized in the following table.

SUMMARY OF SEPARATION ANALYSIS

Test	Data Source	Experimental Results	Stratford's Criterion	Sandborn and Liu's Criterion
1	Schubauer's Air Foil	X = 25.7 ft (7.83 m)	X = 24.2 ft (7.38 m)	X = 25.0 ft (7.62 m)
2	Schubauer's Elliptical Cylinder	X/D = 2.91	X/D = 2.89	X/D = 2.95
3	Roshko's Circular Cylinder	120 to 125 Degrees	100 to 105 Degrees	105 Degrees
4	Yi's Elliptic Afterbody	X = -0.38R	X = -0.45R	X = -0.447R
5	Achenbach's Circular Cylinder	115 Degrees	105 Degrees	110 Degrees

4.0 MISSILE MODELS

In the previous discussion of Stratford's, and Sandborn and Liu's prediction criteria for locating the separation line in turbulent flows, it was pointed out that both methods were derived for two-dimensional, incompressible flow fields. For missiles moving at high angles of attack, the situation is much more complex, because it is basically a three-dimensional, compressible, steady flow pattern. The concentrated vortices break away from the missile on alternate sides in a spatial sense, not in the temporal sense that is normally associated with the classical von Karman vortex street. An illustration of this flow was shown in Figure 2. For the current treatment of this problem, compressibility effects were neglected. It was also postulated that the free stream velocity can be divided into two components which can be treated independently. These were the axial component and the cross flow component. In this analysis, the first step was to relate the angular location of the separation points in the cross-flow planes taken along the axis of the missile model to the axial side force distribution. The second was to obtain two separation lines by connecting the separation points in the cross-sectional planes. The pressure distribution along these two lines was then investigated with respect to the vortex breakaway points and side force variation along the axis. In all calculations, Stratford's separation criterion was used. The required pressure distribution data were made available by AFFDL and AEDC. Details of the experiments and their results are in the following sections.

4.1 AFFDL Data (17)

These data were obtained by Turrelli in the Air Force Flight Dynamics Laboratory's (AFFDL) Trisonic Gasdynamic Facilities (TGF) located at Wright-Patterson Air Force Base in Ohio. The TGF is a closed circuit, variable density, continuous flow wind tunnel, capable of operating within a Mach number range of 0.23 to 4.76, and within a range of unit Reynolds numbers of approximately 0.25×10^6 to 5.85×10^6 per foot. The model used in this experiment consisted of a sharp, tangent ogive nose followed by a cylindrical afterbody of one inch in diameter. A sketch of the model is shown in Figure 11. Pressure data were measured with 84 pressure orifices located at six axial stations of the cylindrical portion of the model, as shown in Figure 12. The six axial stations were located at 3.5 to 7.0 model diameters aft of the nose tip. The free stream Mach number was 0.3 for the data used in the current calculations. The angles of attack were 40 and 45 degrees, and the Reynolds number was kept at 2.0×10^6 per foot. A nose boundary layer trip was placed at 1.25 to 1.75 inches aft of the nose tip, and only on one side of the model in order to force a steady asymmetrical vortex pattern. It is interesting to note that no significant side forces were measured with the smooth model. Two curves of pressure distribution at 3.5R aft of the model nose tip with/without the grit are shown in Figure 13 and Figure 14. These curves were obtained by connecting the measured data points with smooth curves. Data used in the current calculations were interpolated along the curves at 5-degree increments. Figure 15 shows

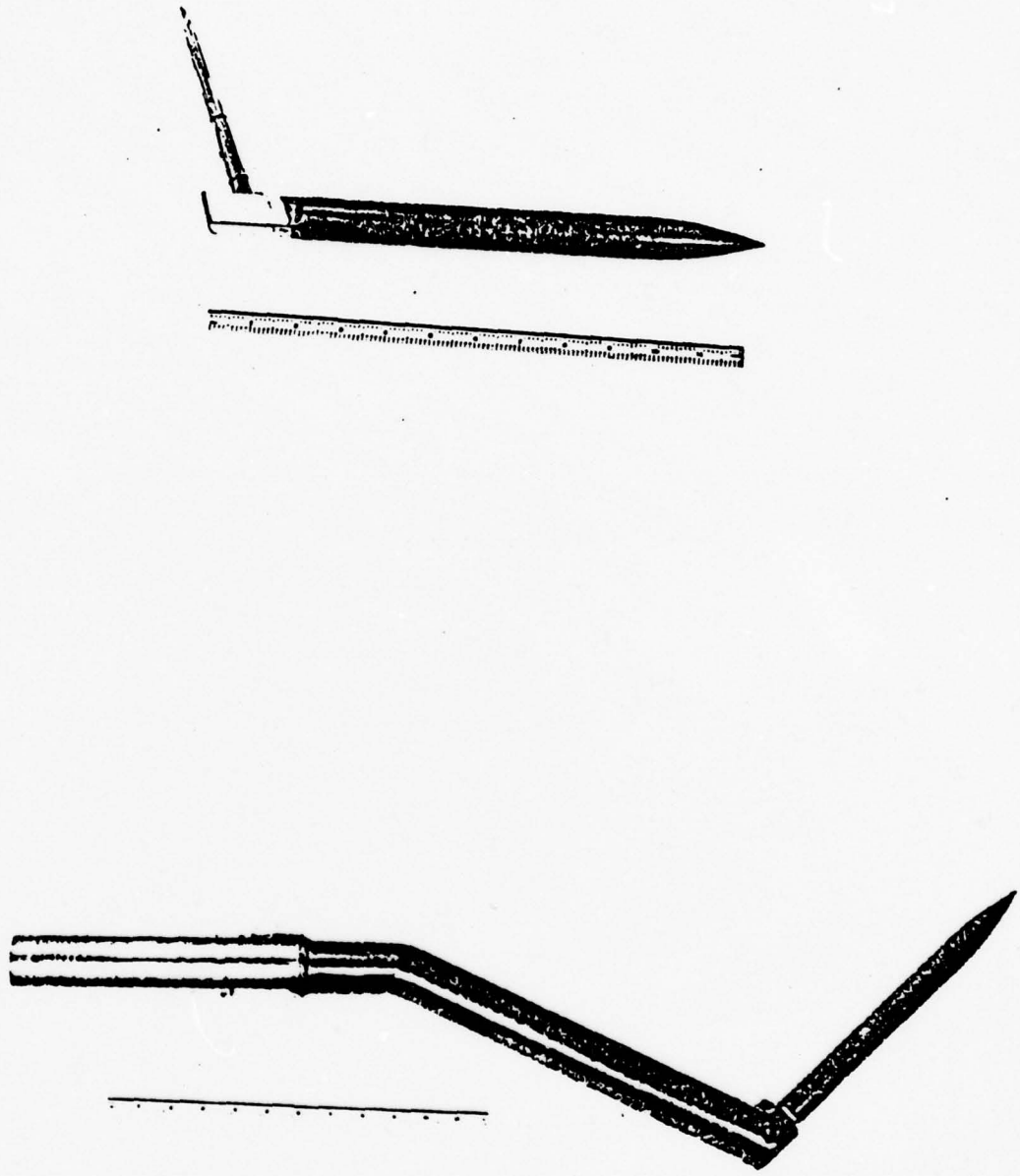

FIGURE 11 AFFDL MISSILE MODEL

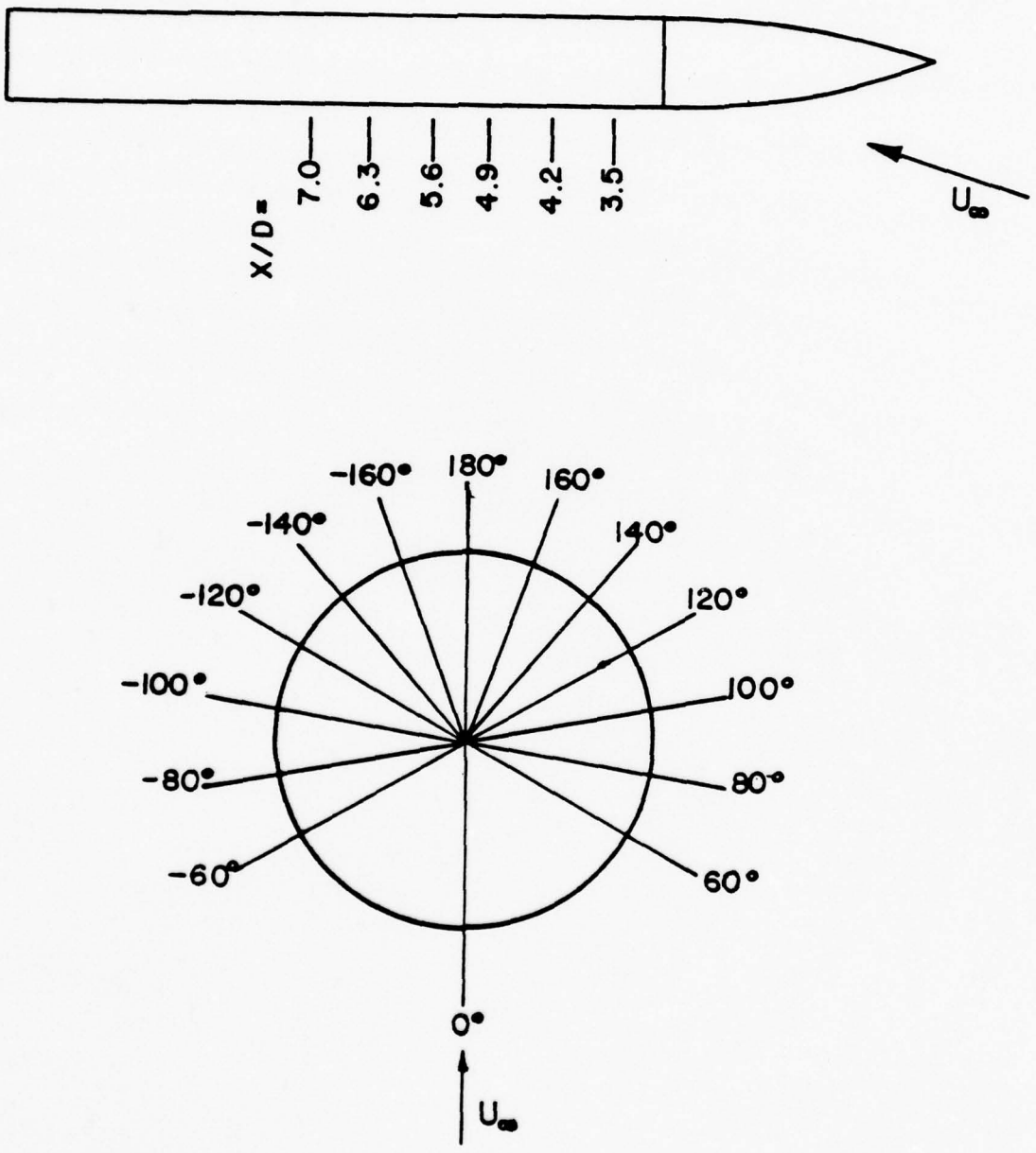

FIGURE 12 LOCATION OF PRESSURE TAPS ON AFFDL MODEL

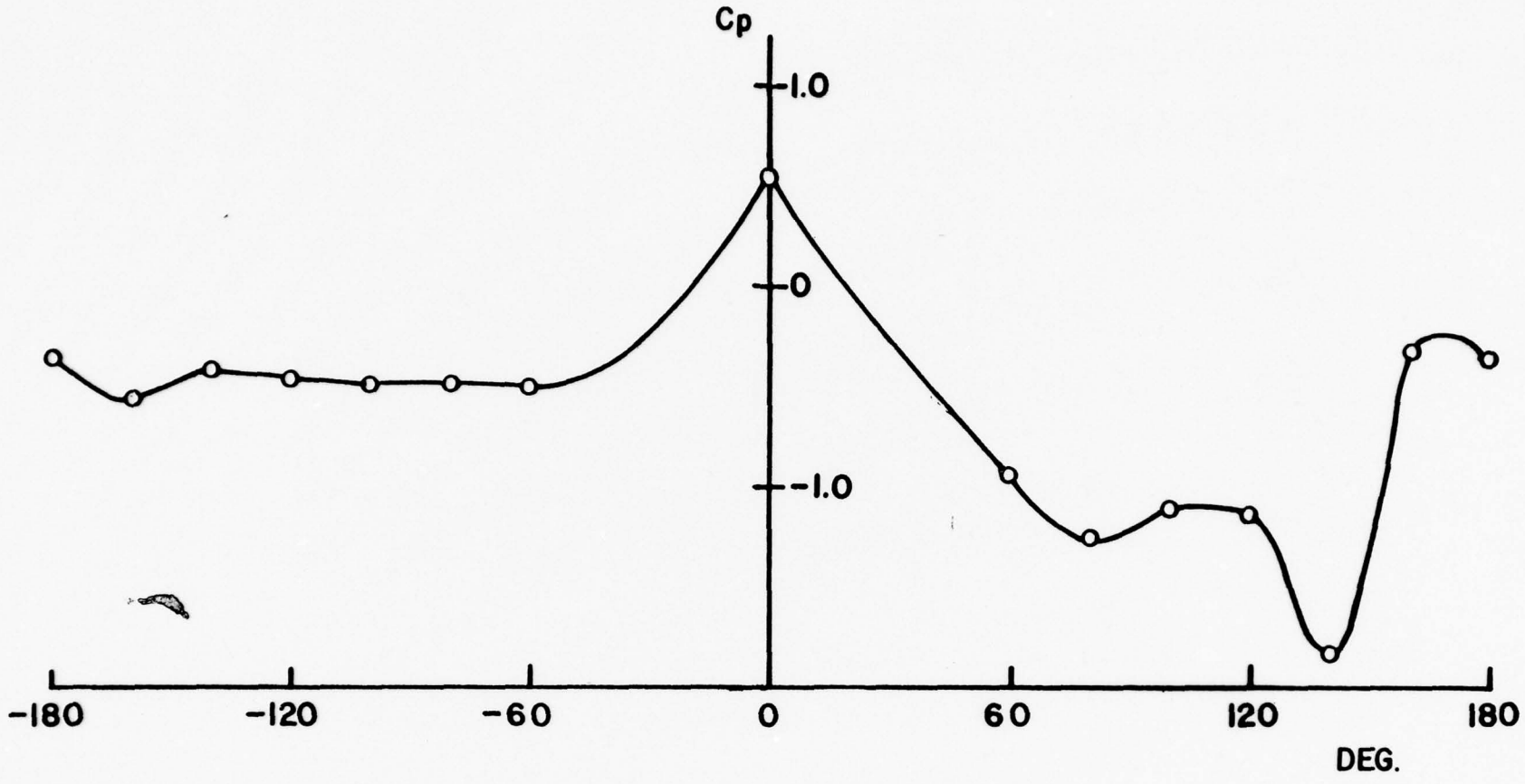

FIGURE 13 PRESSURE DISTRIBUTION
(X/D=3.5, M=0.3, α=45°, W/ GRIT)

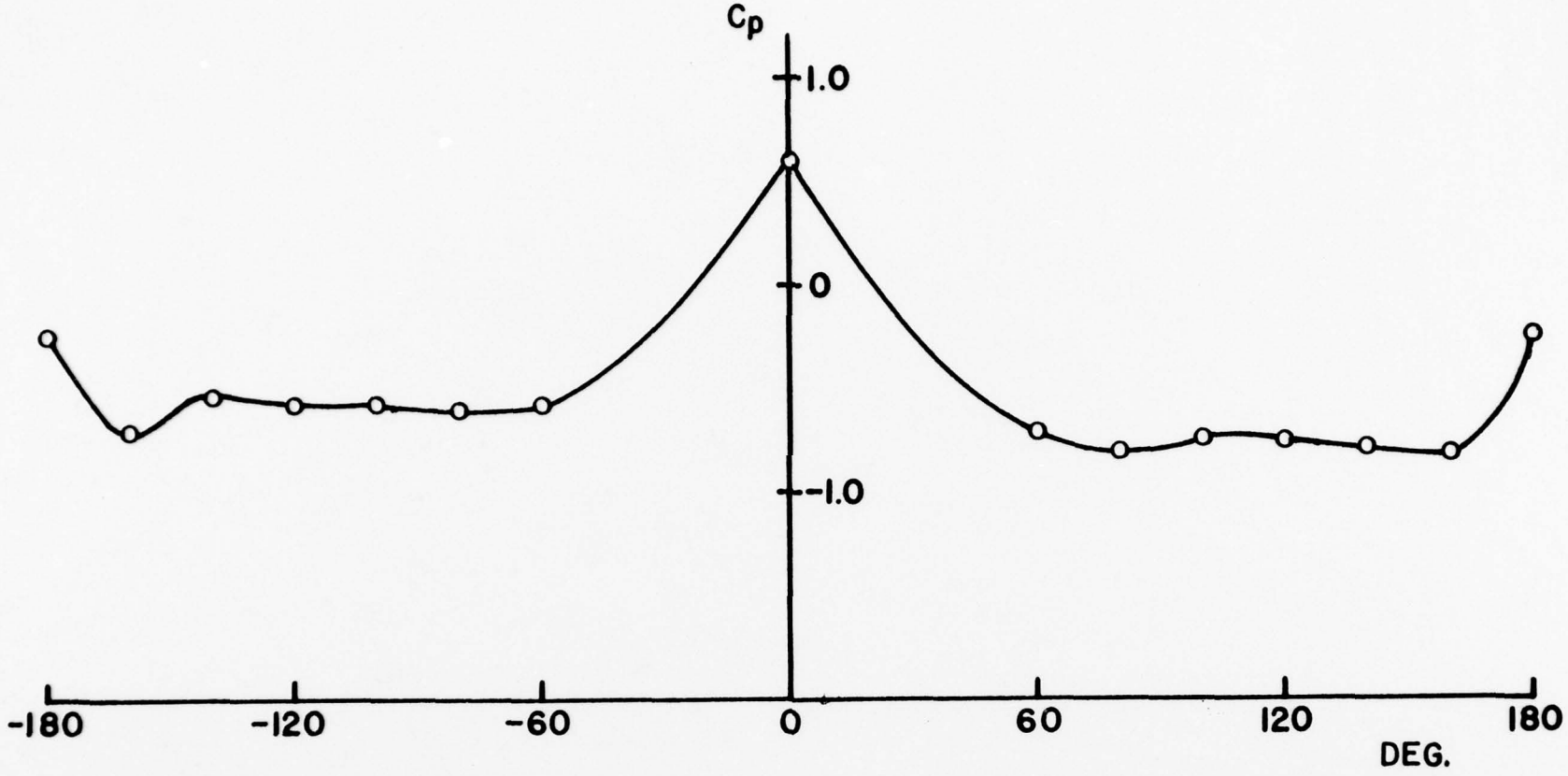

FIGURE 14 PRESSURE DISTRIBUTION
(X/D=3.5, M=0.3, α=45°, W/O GRIT)

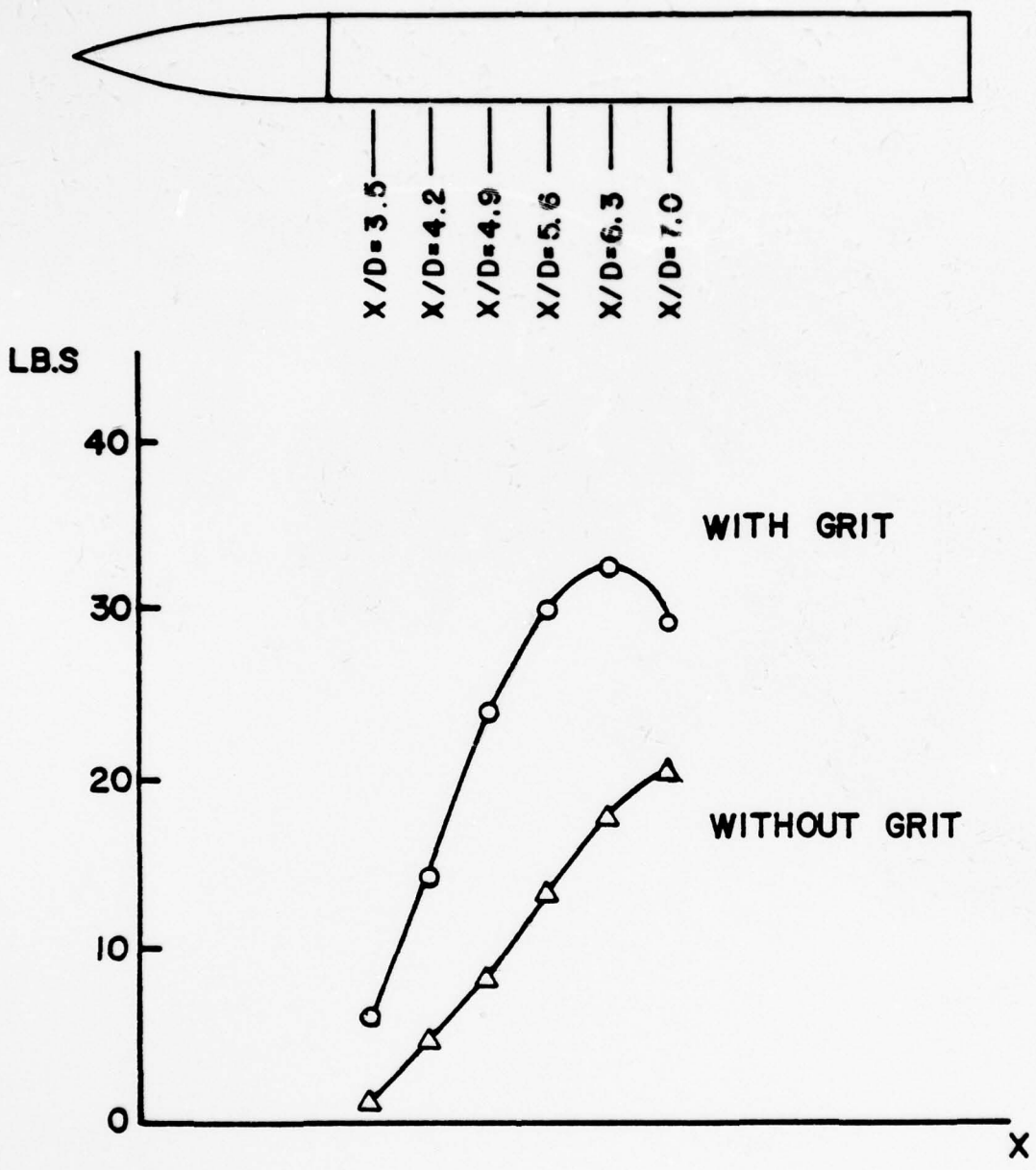

FIGURE 15 SIDE FORCE DISTRIBUTION
($M=0.3$, $Re=2\times10^6$, $\alpha=45°$)

the side force distribution at M = 0.3, Re = 2 x 10^6/ft., 45 degree angle of attack, and with grit, and also shows the same condition but without grit. No measurements were made between zero and 60 degrees on the windward side of the model. The results of applying Stratford's separation criterion were very inconsistant. The basic problem with the calculation was the lack of more detailed information on the pressure distribution. The data interpolation was probably not representative of the real flow.

Two flow visualization techniques were applied in this experiment. A Z-type Schlieren system was used to view the flow field patterns and vortex lines, and an oil flow technique was used to observe the interaction of surface streamlines and regions of flow separation. Schlieren photographs did not show the locations of the trailing vortices due to the very small density gradients. However, flow separation was observed between the 85 to 95 degree points on the model over its entire length for all test conditions. In view of the above problems and data uncertainties, no further analysis of these experimental data was pursued.

4.2 AEDC Data

These tests were conducted in the propulsion wind tunnel at Arnold Engineering Development Center (AEDC), Tennessee. This wind-tunnel is a close circuit, continuous flow type tunnel capable of operating at Mach numbers from 0.2 to 1.6. The model used in the tests represents an 11.57 percent model of the MX3-80 missile. Details of the model and sting support are shown in Figure 16, and the ogive nose details are

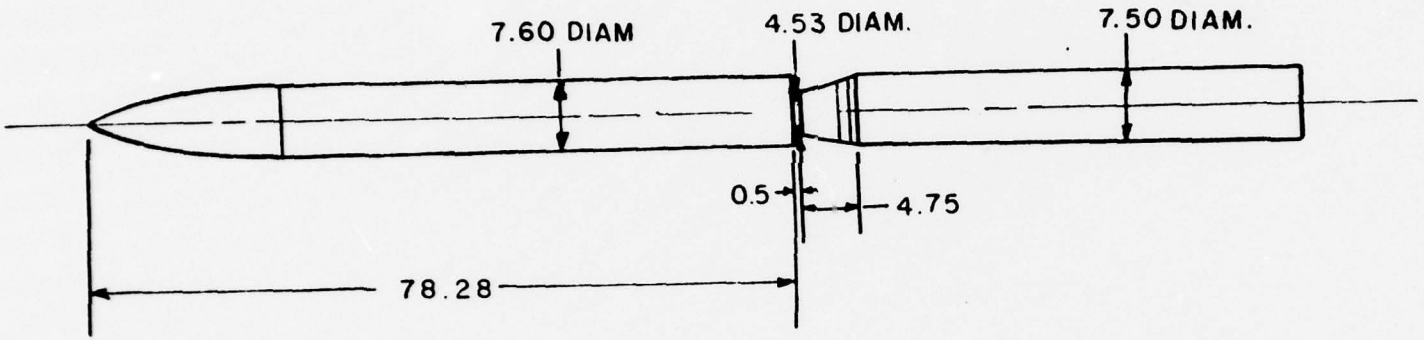

DIMENSIONS IN INCHES

FIGURE 16 AEDC MODEL AND SUPPORT

shown in Figure 17. Pressures were measured at 14 locations along the model. At each location either 16 or 22 pressure orifices were installed, as shown in Figure 18. Two sets of data were utilized in the current calculations. They were measured at a Mach number of 0.4, at a Reynolds number of 2.0×10^6 per foot. Angles of attack were 40 degrees and 45 degrees, and the roll angles were 45 degrees and 0 degrees, respectively. For an angle of attack of 45 degrees, the wake flow field was surveyed at model station 30 inches (76.2 cm), 53.2 inches (135.1 cm), and 70.0 inches (177.8 cm) from the nose. These corresponded to X/D values of 3.95, 7.0, and 9.2, repsectively. For an angle of attack of 45 degrees, two wake surveys were obtained at X/D = 7.0 and 9.2. The positions where the vortices left the model surface were determined by plotting the measured vortex cores. By connecting the core position with a straight line and extrapolating back to the missile surface, the vortex breakaway points were estimated. The breakaway points of the remaining vortices in the field were estimated by extrapolating their positions back to the missile surface along a line parallel to the one determined by the two vortex centers of like sign. Figure 19 and Figure 20 illustrate the results of this procedure.

In order to obtain a better physical understanding of the vortex development, color Schlieren photographs of flow fields associated with a series of sharp-nosed models were obtained in the Rutgers Emil Buehler Wind Tunnel. The angle of attack of the models could be varied over a range of angles of attack. Figure 21 shows a typical flow field.

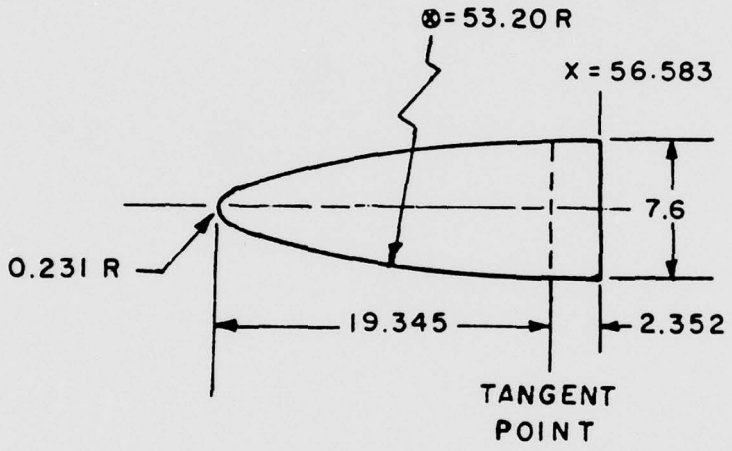

DIMENSIONS IN INCHES

FIGURE 17 AEDC MODEL — NOSE DETAIL

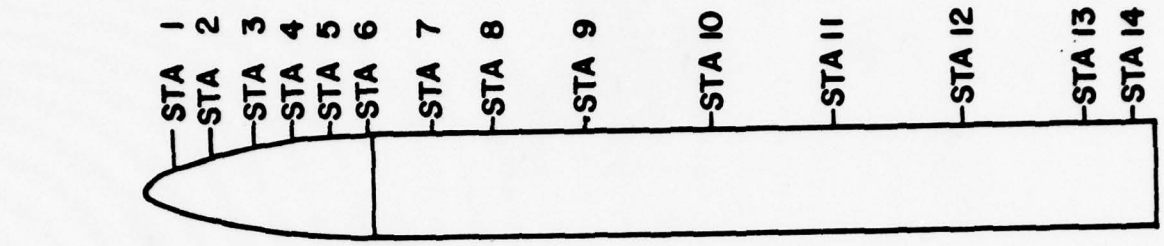

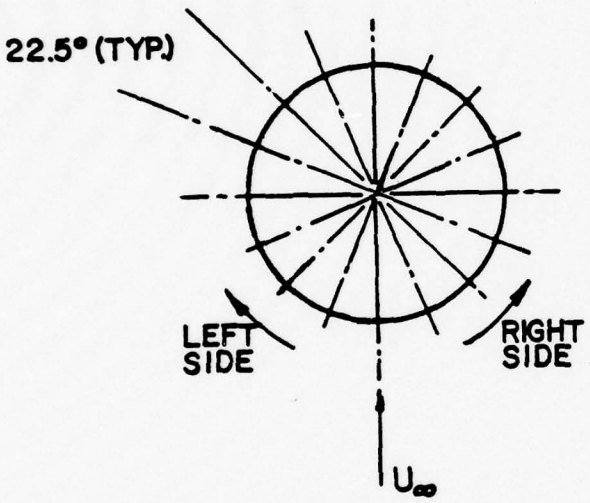

PRESSURE ORIFICE LOCATION, 16 EACH (STA. 1,2,4,6,9,11,12,13)

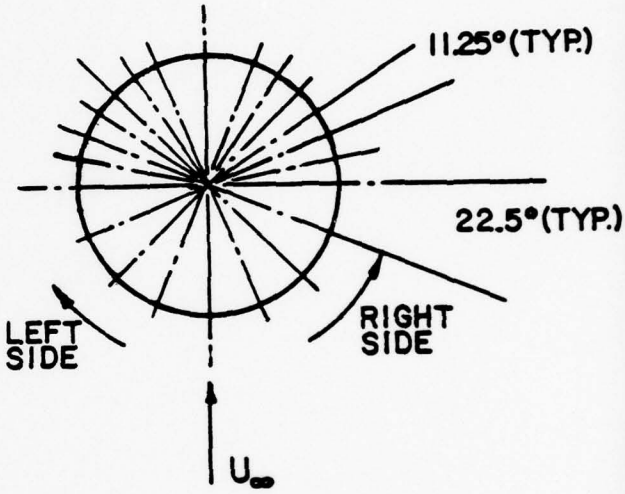

PRESSURE ORIFICE LOCATION, 22 EACH (STA. 3,5,7,8,10,14)

FIGURE 18 LOCATION OF PRESSURE TAPS (AEDC MODEL)

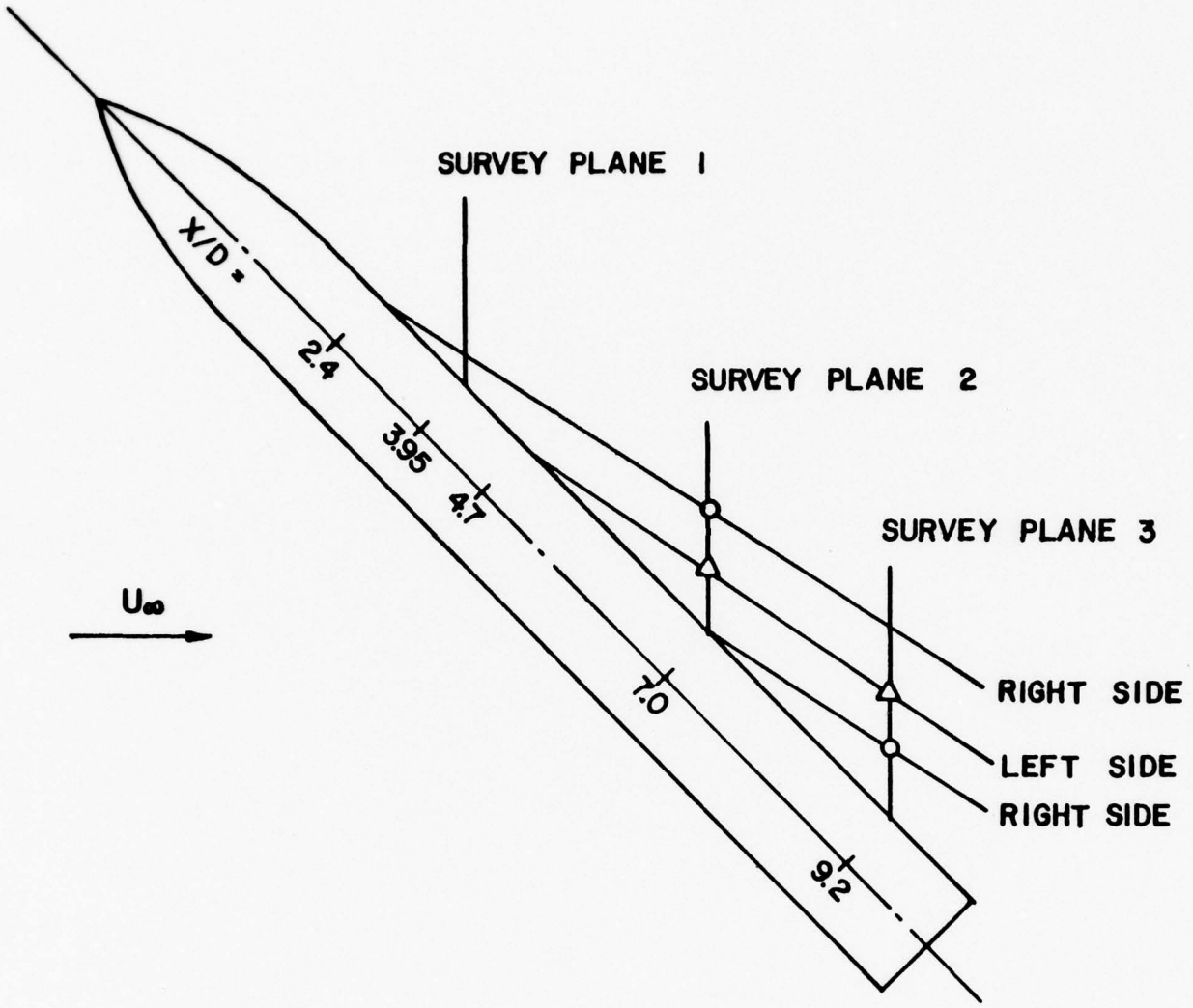

FIGURE 19 VORTEX "BREAKAWAY" LOCATIONS
M=0.4, α=45°, ϕ=0°

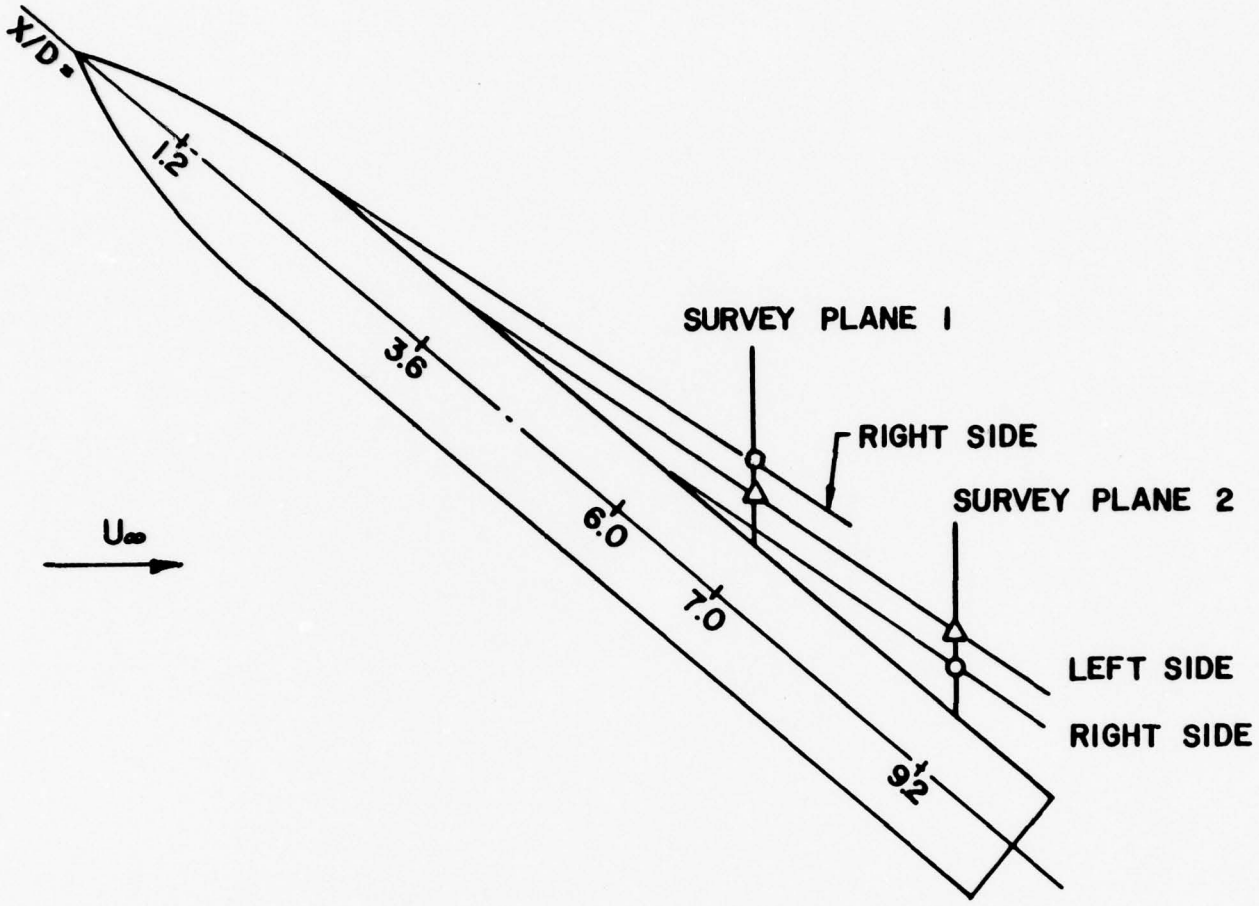

FIGURE 20 VORTEX "BREAKAWAY" LOCATIONS
M=0.4, α=40°, ϕ=45°

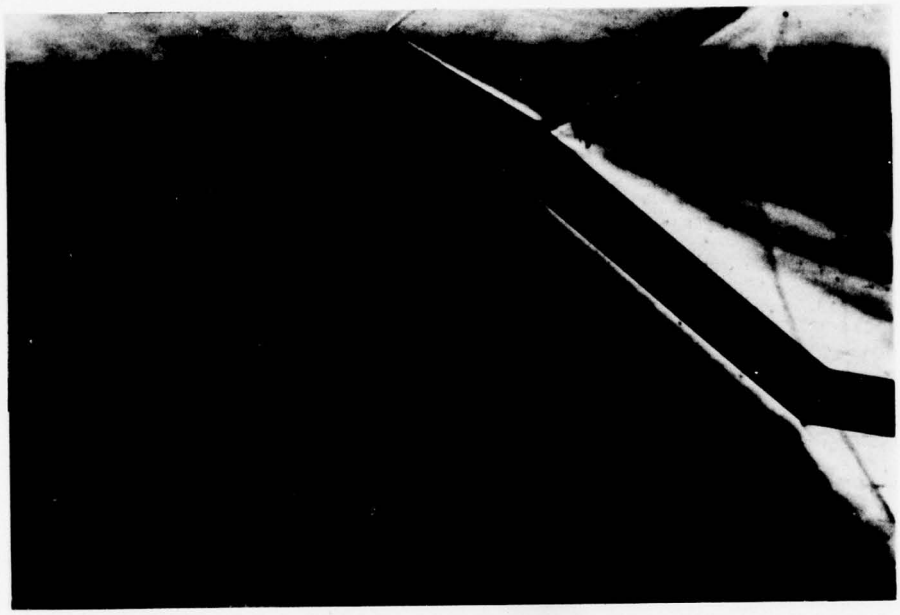

Flow Conditions: $M_\infty = 1.04 \quad \alpha = 41^\circ$

FIGURE 21 SCHLIEREN PHOTOGRAPH

4.3 Analysis of AEDC Data

As indicated in Section 2.1, Stratford's formula is only valid in the region of a positive pressure gradient following the point of maximum dynamic pressure. In applying Stratford's method to the two sets of pressure data, separation was predicted for some of the stations taken along the axis of the model. For those stations where Stratford's model failed to predict separation, the C values in Stratford's equation were very close to the lower boundary of the criterion, i.e., 0.35. Since the pressure data were taken at relatively large increments, i.e., 22.5 degrees, it was again very difficult to determine the behavior of the pressure curve following the point of relative mimimum pressure. The two sets of data were nevertheless plotted and connected with smooth curves. By examining the adverse pressure gradients on these curves, separation points were estimated for the stations where Stratford's method did not predict separations. Figure 22 through Figure 25 are the pressure distribution curves at stations 1 and 8 for both sets of data. The angular locations of separation points on both sides of the model were plotted in Figure 26 through Figure 29. The pressure coefficient, C_p, of these separation points was then plotted in the axial direction, as shown in Figure 30 through Figure 33. In Figure 34 and Figure 35, side force distribution along the model axis were plotted for both sets of data. These graphs were studied with respect to the vortex breakaway points.

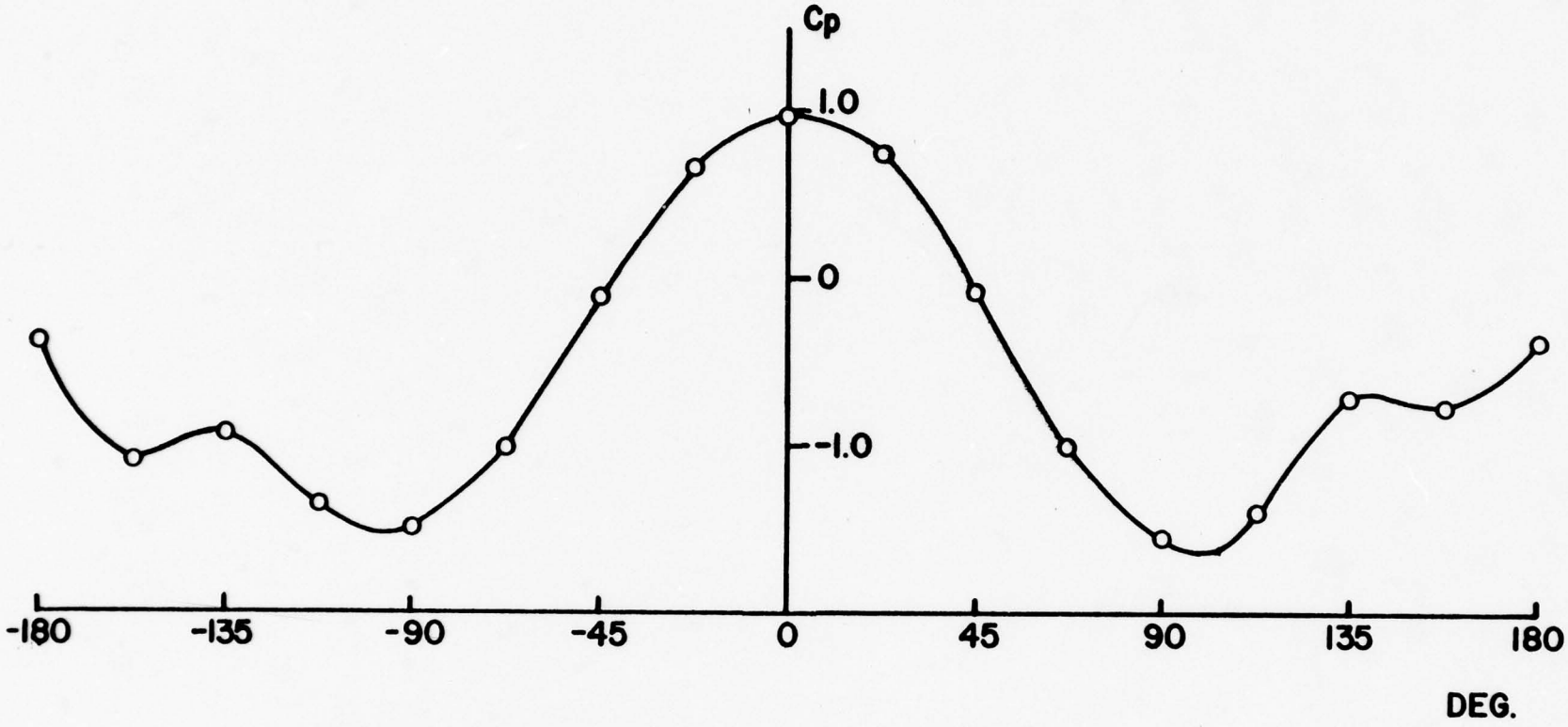

FIGURE 22 PRESSURE DISTRIBUTION
STATION 1, M=0.4, α=45°, ϕ=0°

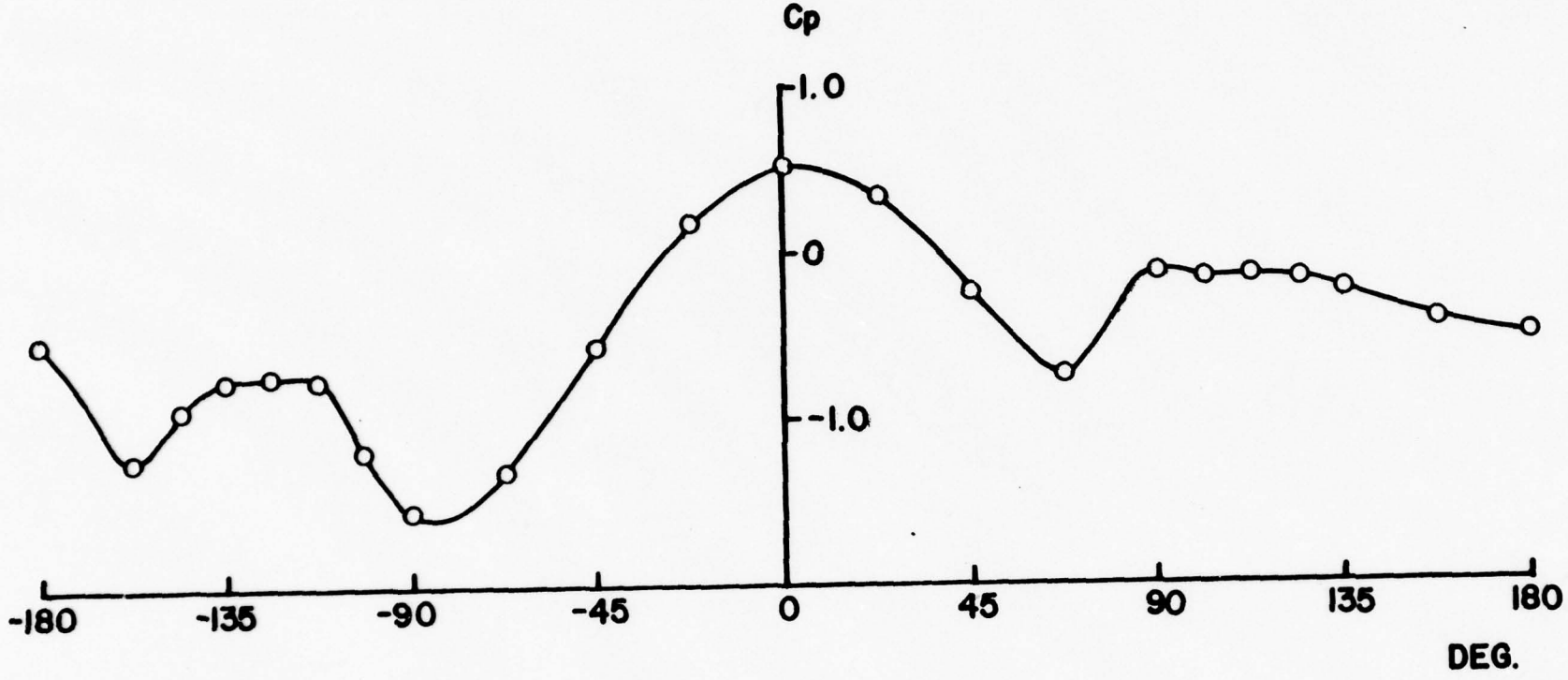

FIGURE 23 PRESSURE DISTRIBUTION
STATION 8, M=0.4, α=45°, ϕ=0°

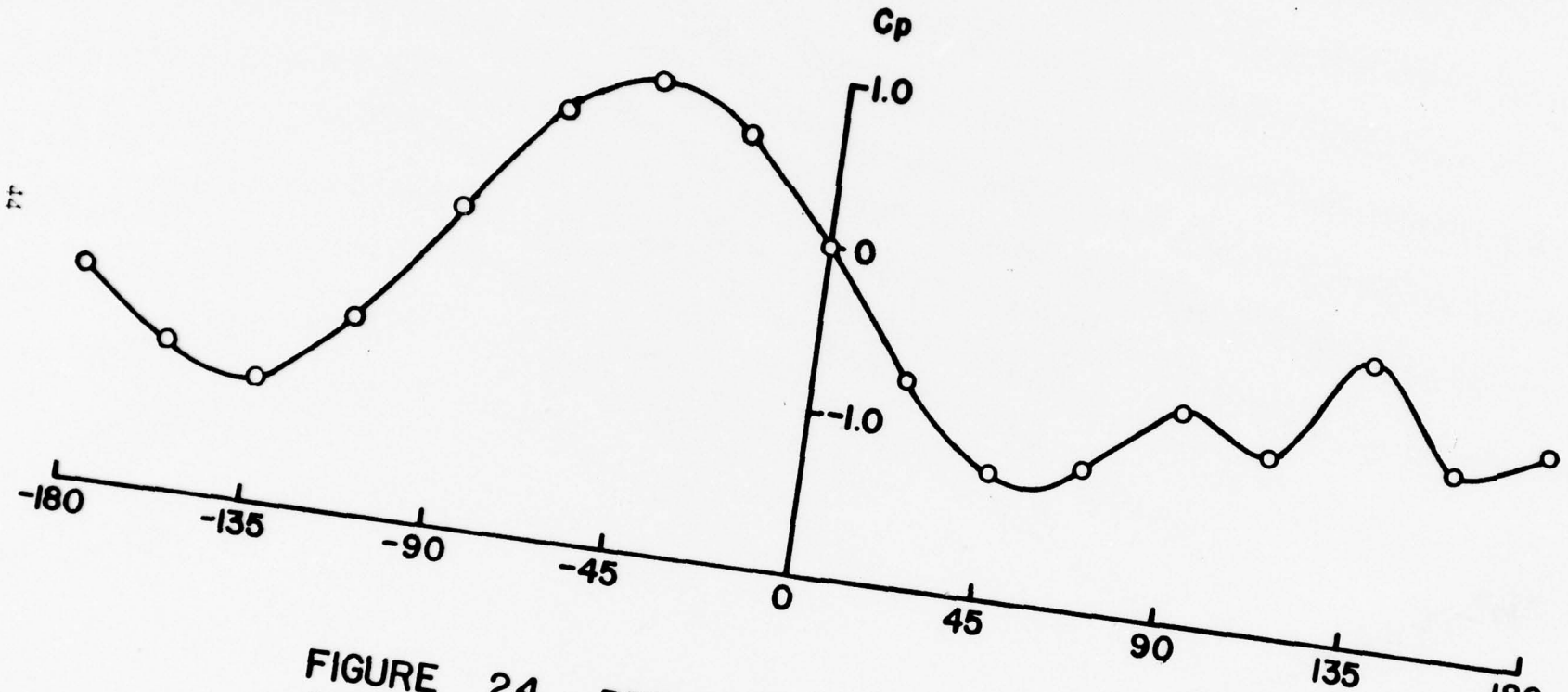

FIGURE 24 PRESSURE DISTRIBUTION
STATION 1, M=0.4, α=40°, ϕ=45°

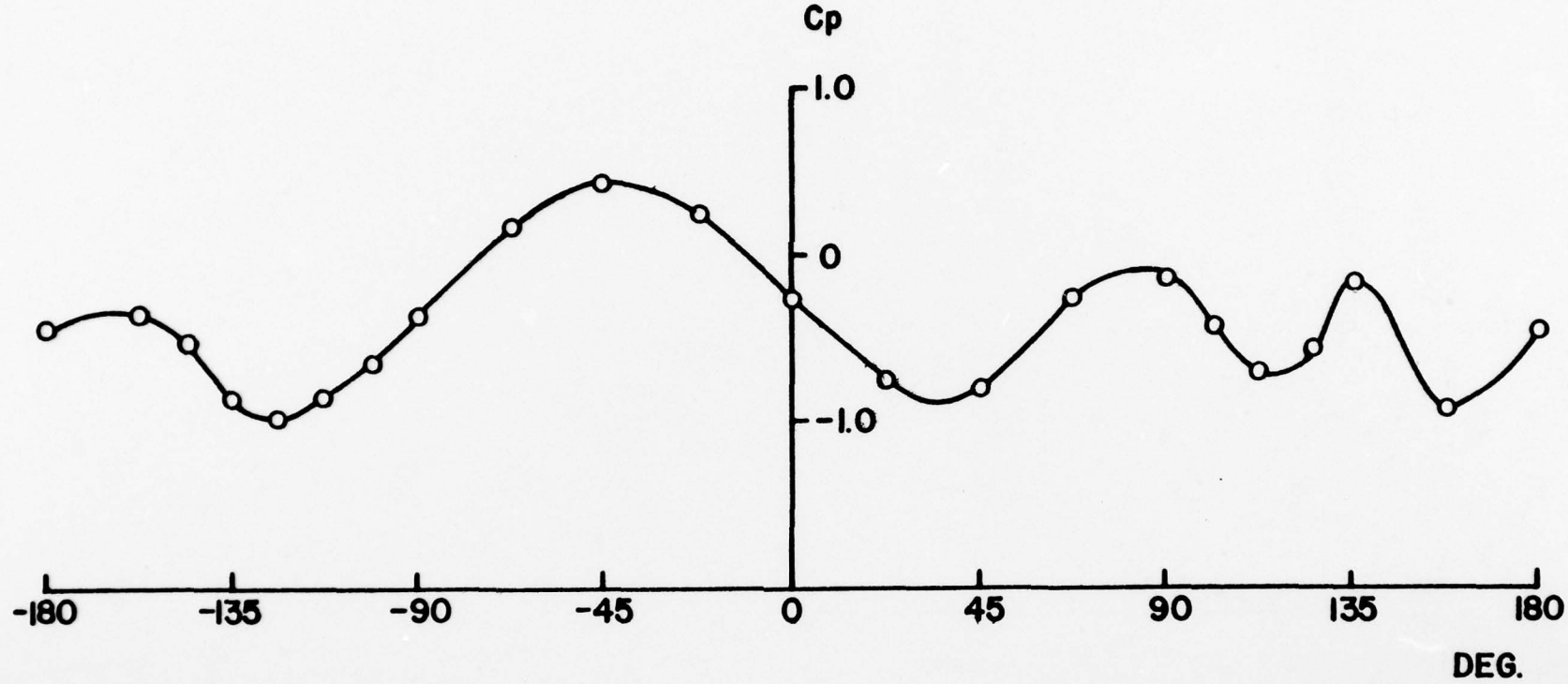

FIGURE 25 PRESSURE DISTRIBUTION
STATION 8, M=0.4, α =40°, ϕ =45°

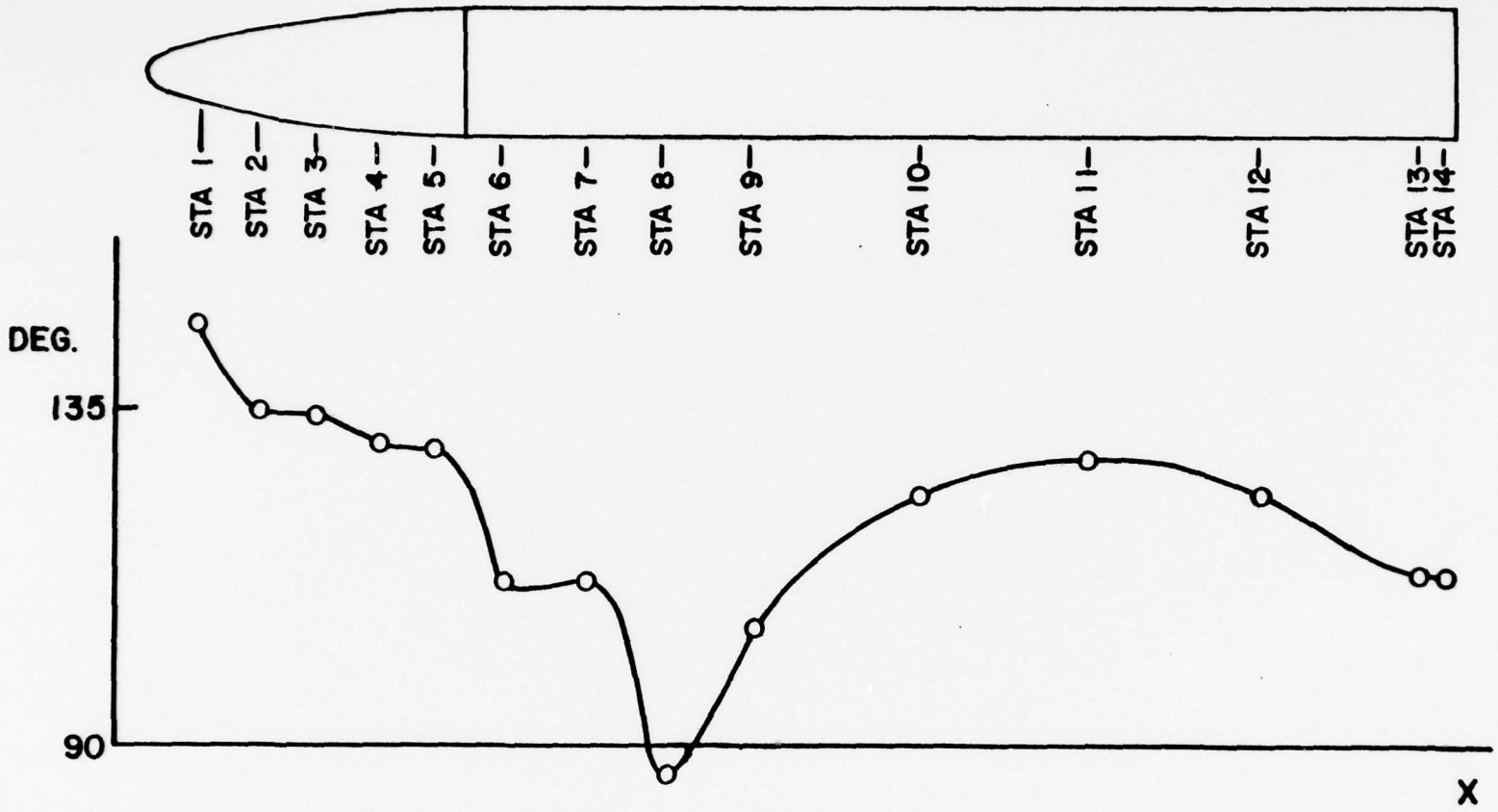

FIGURE 26 SEPARATION LOCATIONS
(LEFT SIDE, M=0.4, α=45°, ϕ=0°)

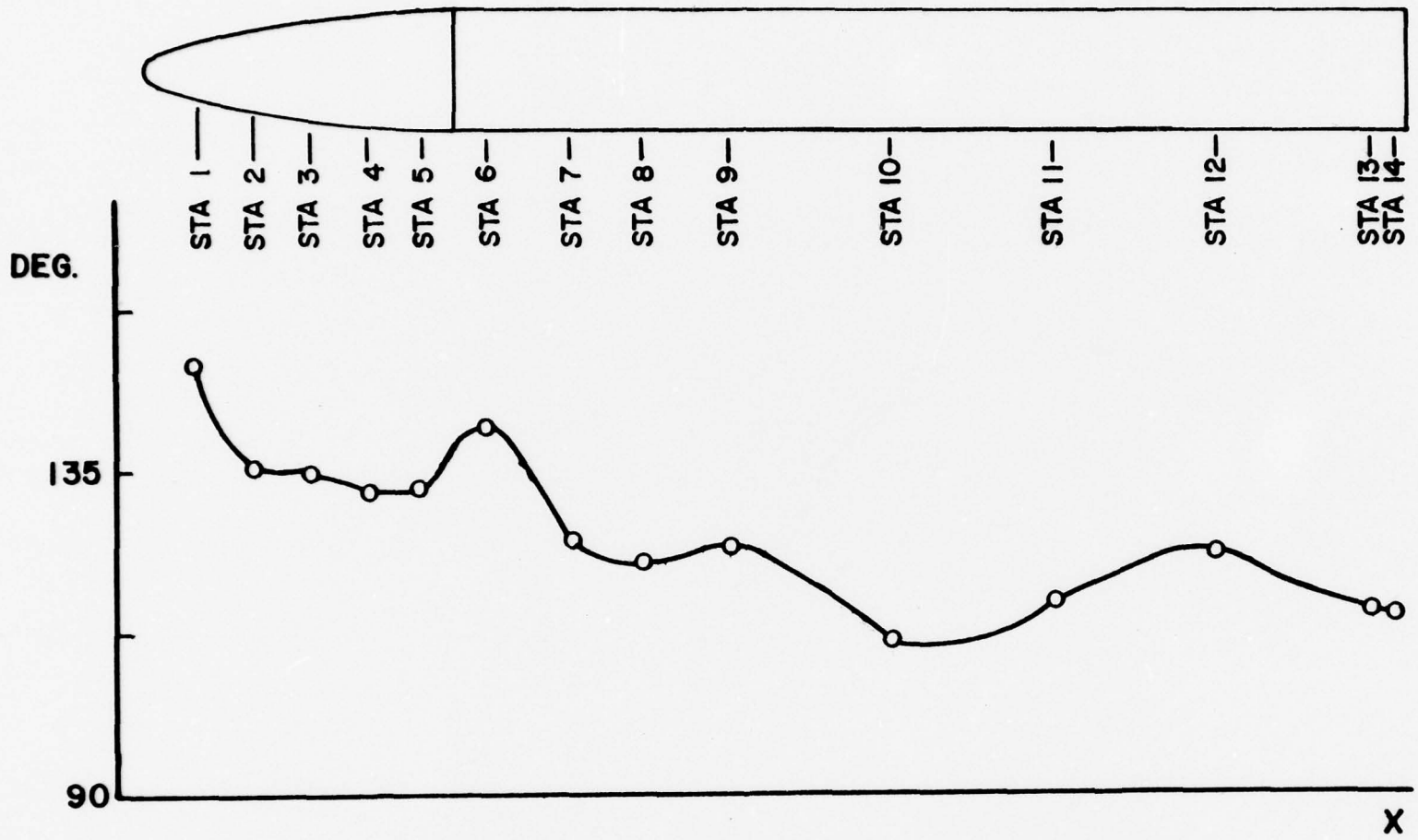

FIGURE 27 SEPARATION LOCATIONS
(RIGHT SIDE, M=0.4, α=45° ϕ=0°)

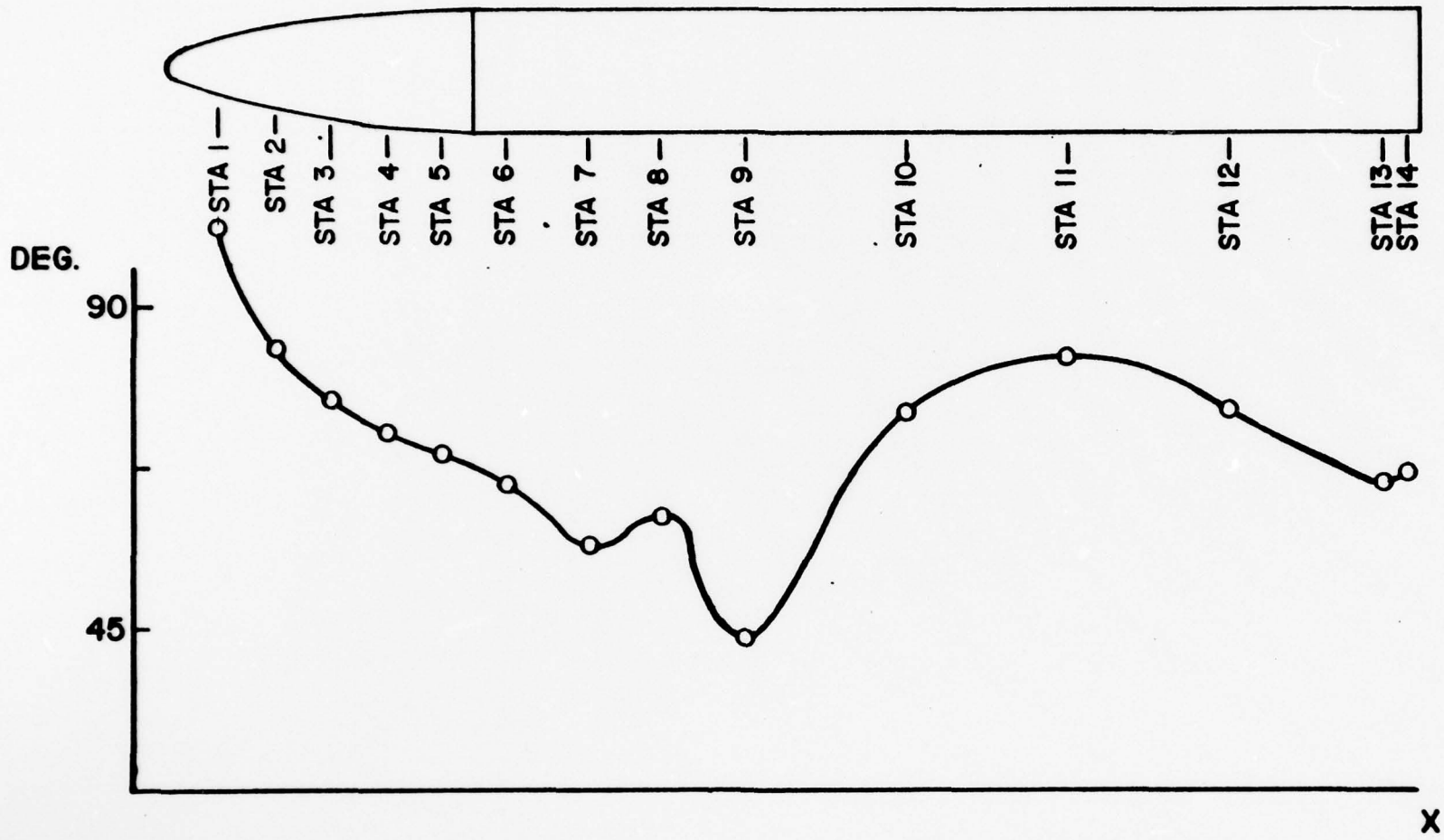

FIGURE 28 SEPARATION LOCATIONS
(LEFT SIDE, M=0.4, α=40°, ϕ=45°)

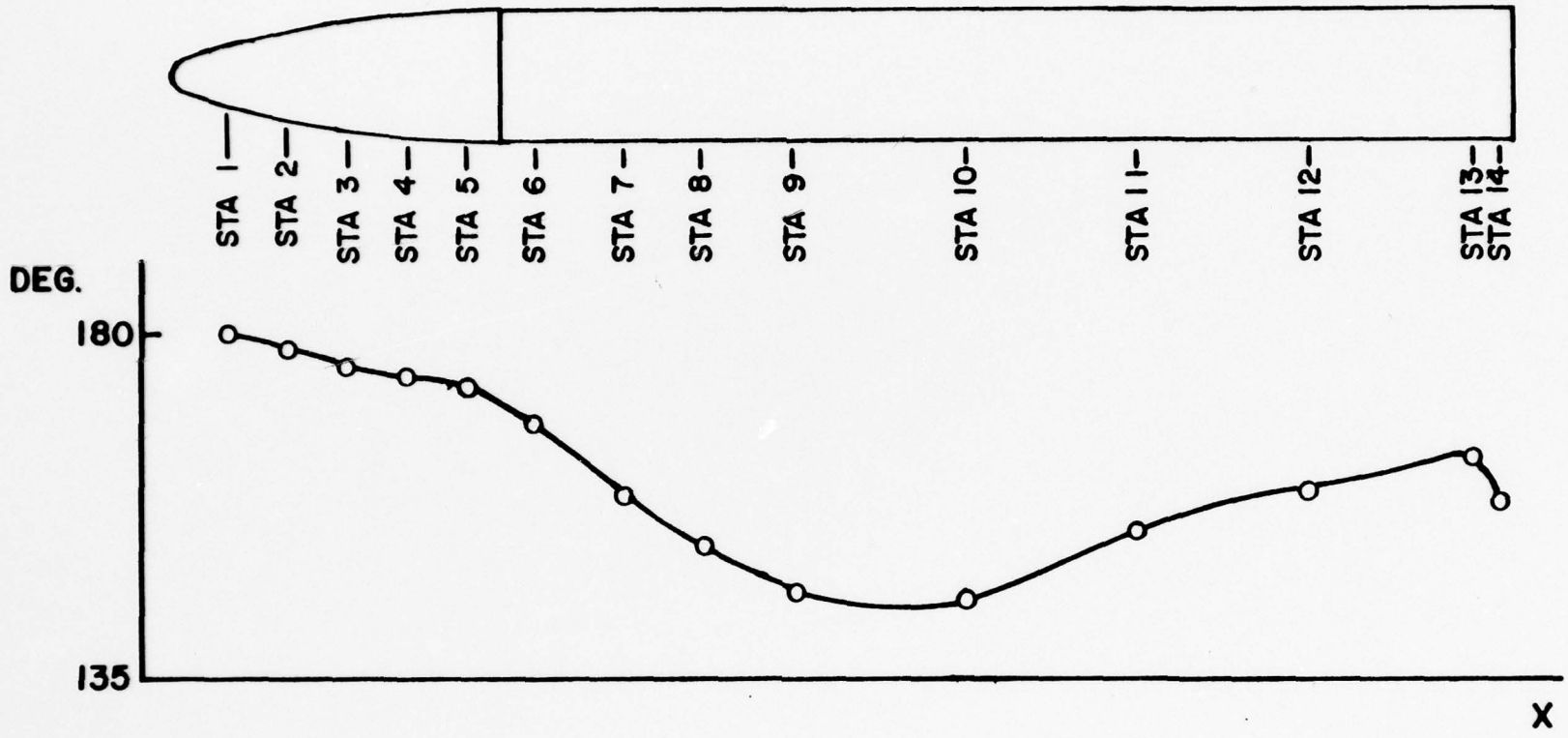

FIGURE 29 SEPARATION LOCATIONS
(RIGHT SIDE, M=0.4, α=40°, ϕ=45°)

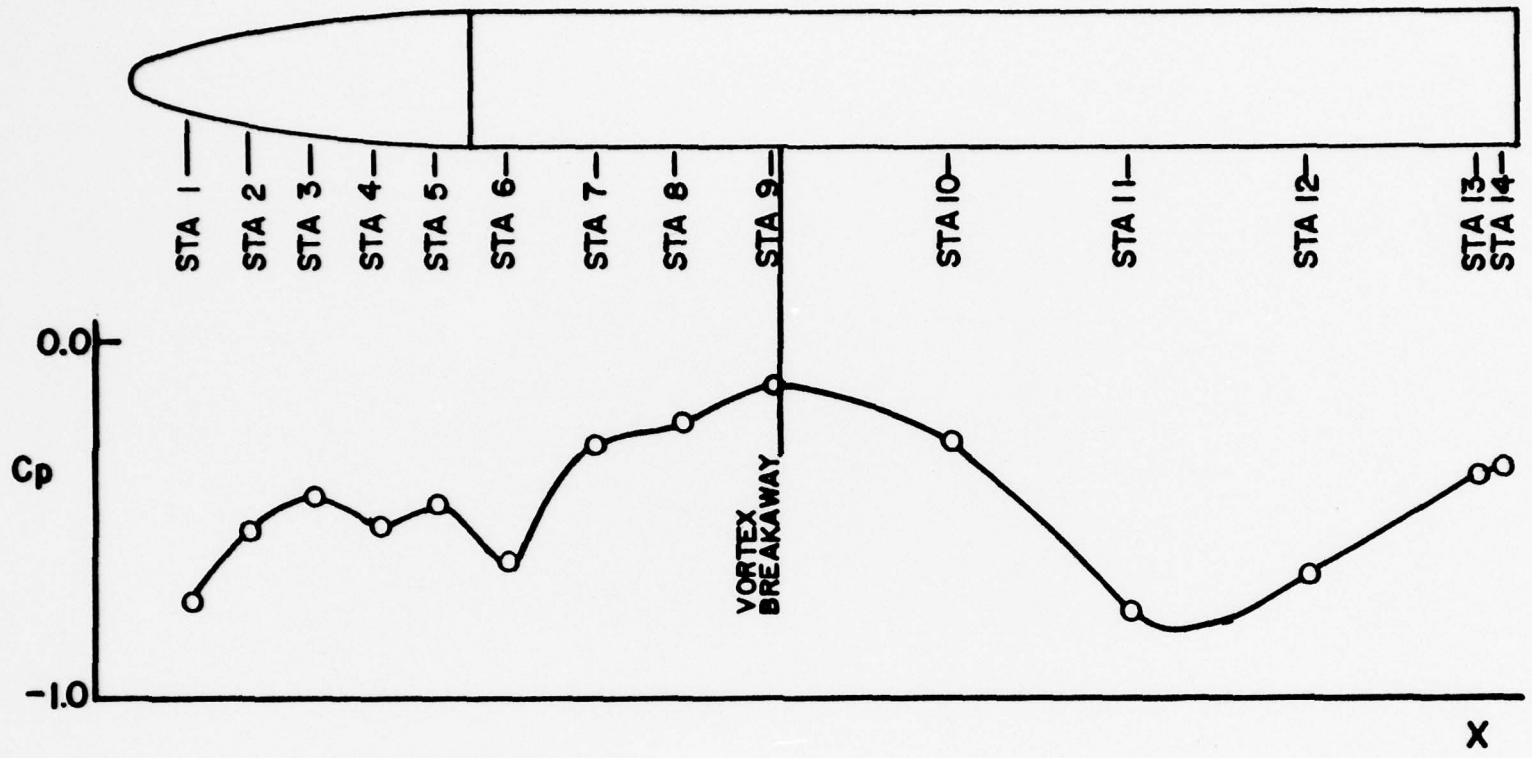

FIGURE 30 AXIAL PRESSURE DISTRIBUTION
(LEFT SIDE, M=0.4, $\alpha = 45°$, $\phi = 0°$)

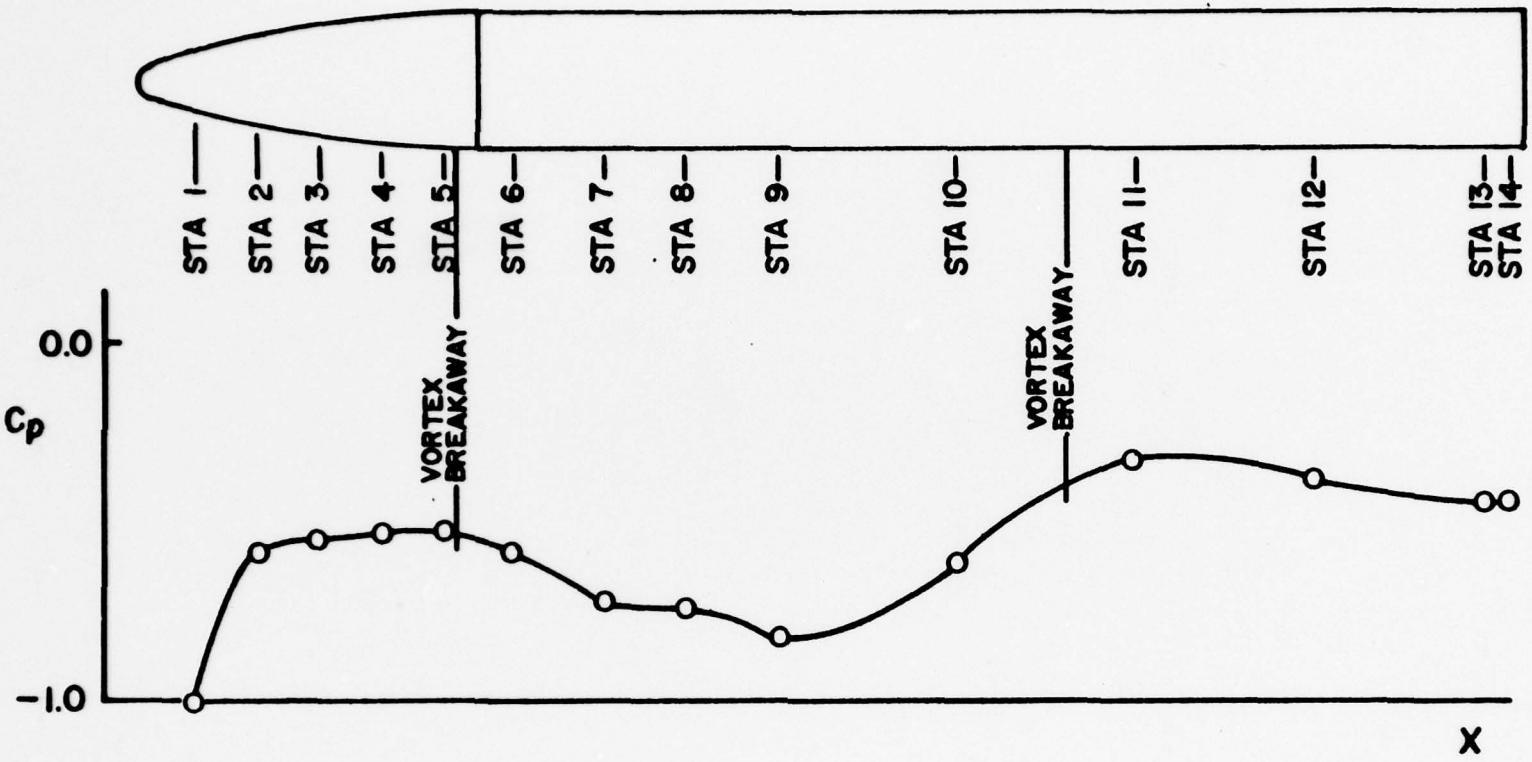

FIGURE 31 AXIAL PRESSURE DISTRIBUTION
(RIGHT SIDE, M=0.4, $\alpha = 45°$, $\phi = 0°$)

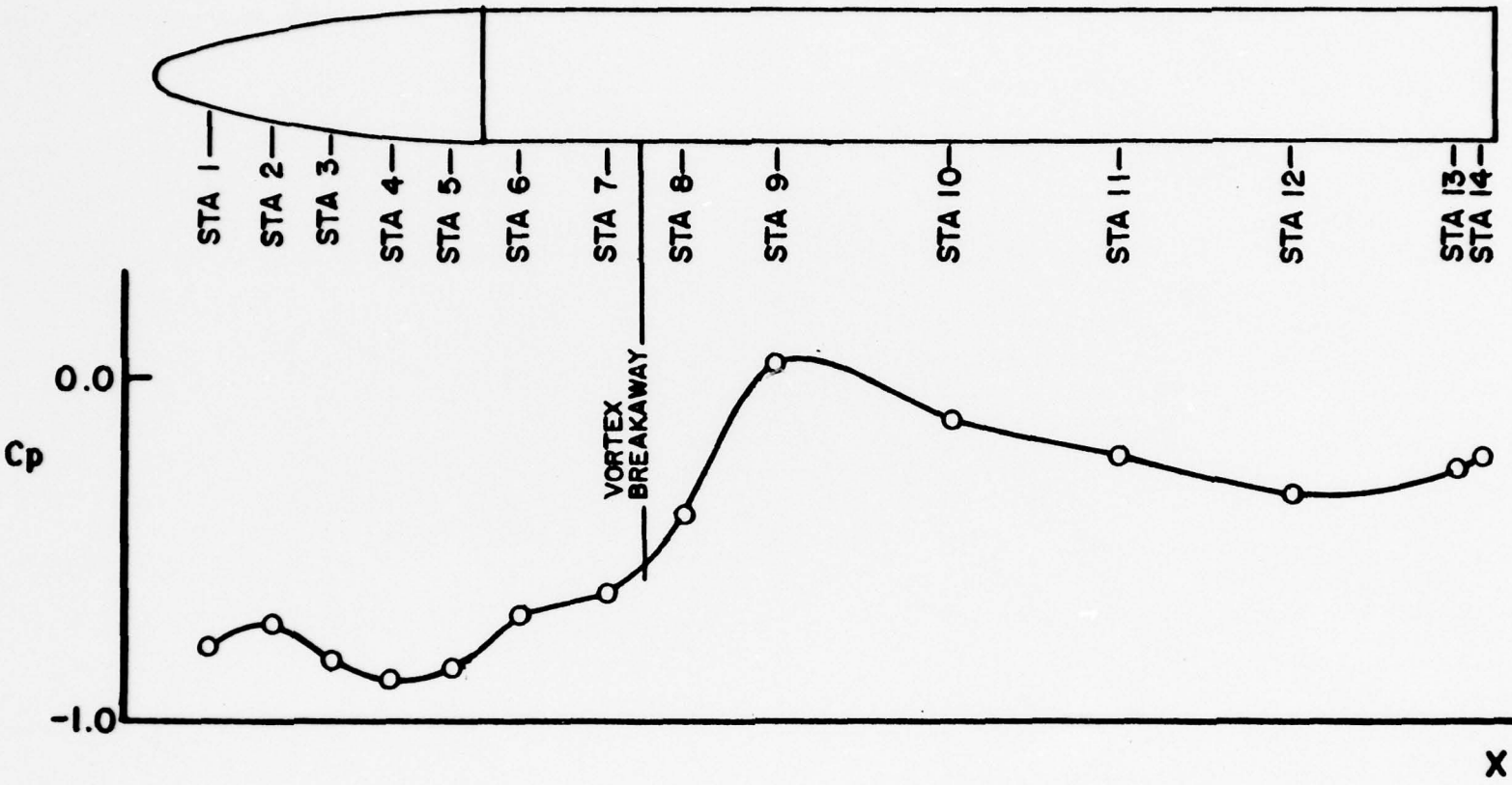

FIGURE 32 AXIAL PRESSURE DISTRIBUTION
(LEFT SIDE, M=0.4, α=40°, ϕ=45°)

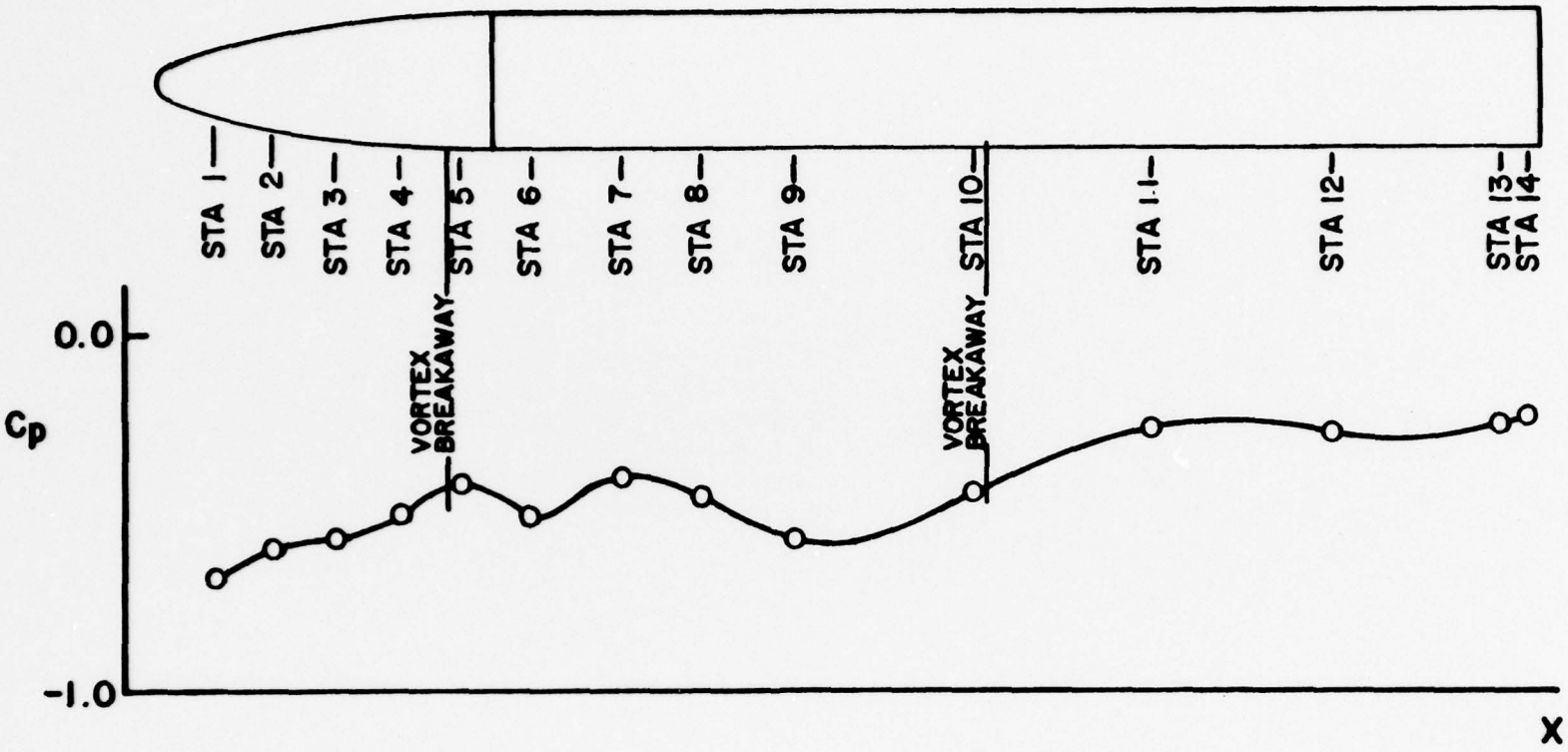

FIGURE 33 AXIAL PRESSURE DISTRIBUTION
(RIGHT SIDE, M=0.4, α=40°, ϕ=45°)

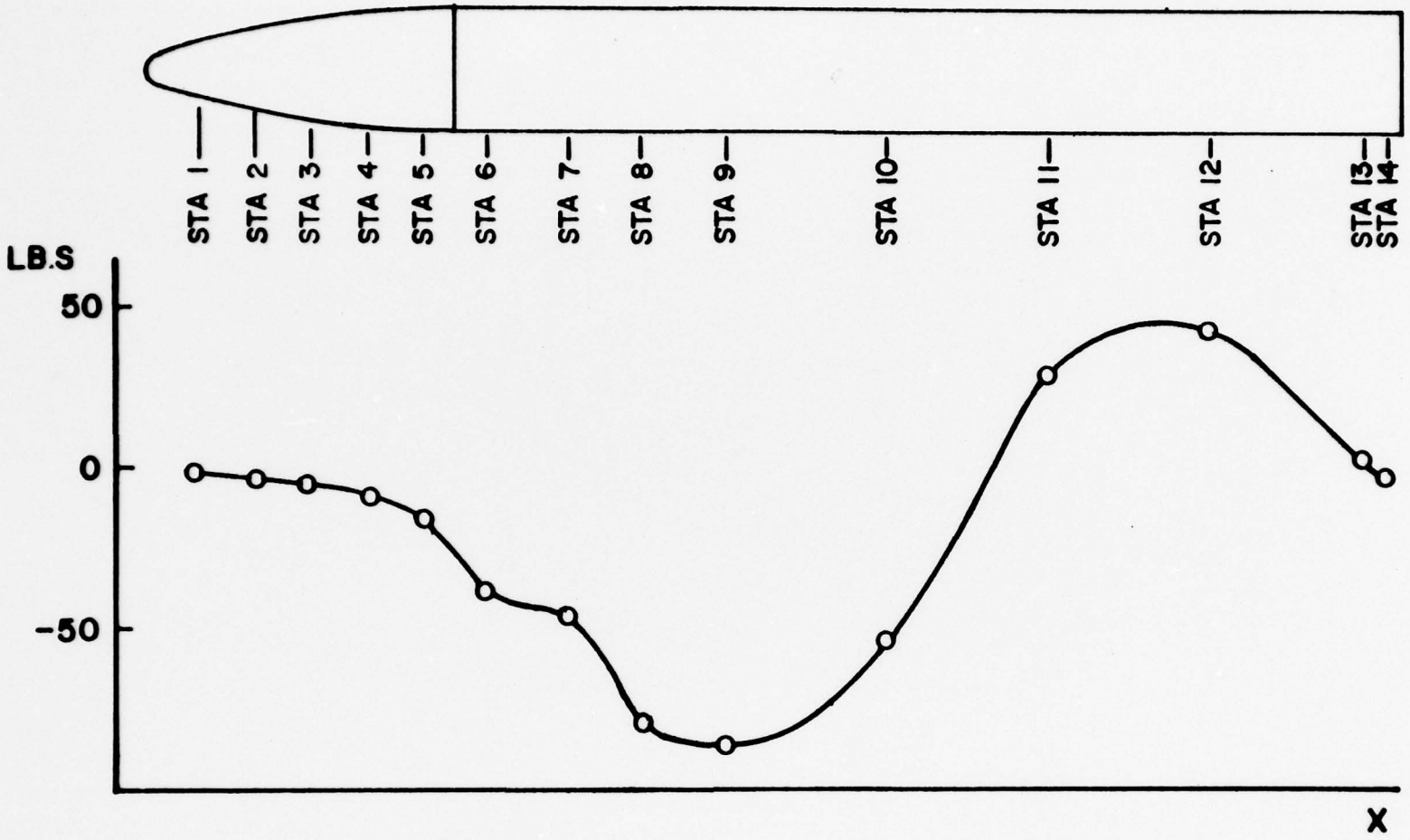

FIGURE 34 SIDE FORCE DISTRIBUTION
(M=0.4, α =45°, ϕ=0°)

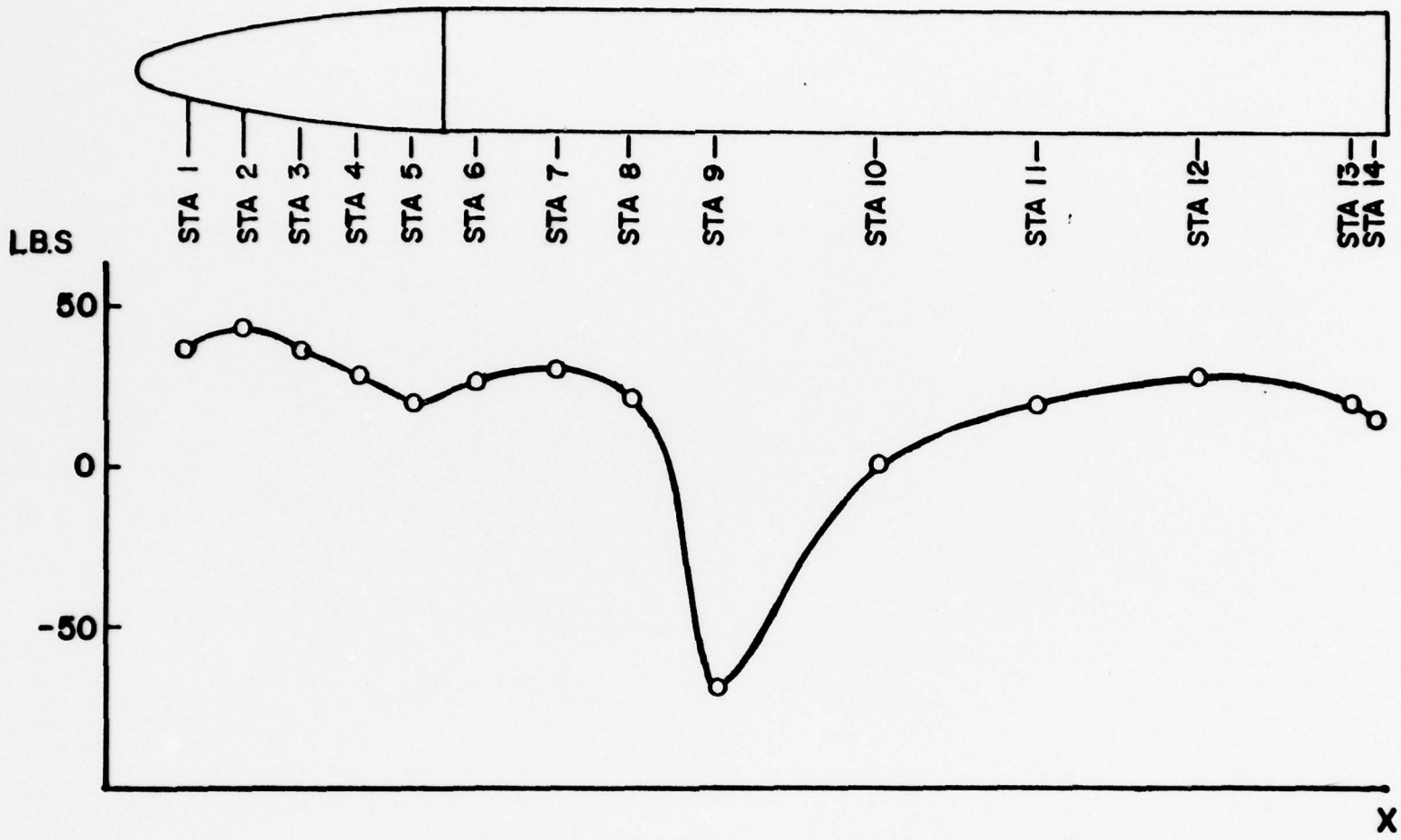

FIGURE 35 SIDE FORCE DISTRIBUTION
(M=0.4, $\alpha = 40°$, $\phi = 45°$)

5.0 RESULTS AND DISCUSSION

For the first set of AEDC data ($M = 0.4, \alpha = 45$ degrees, $\phi = 0$ degrees), it was found that near the nose and the tail of the missile model, the flow pattern was almost symmetrical with respect to the free stream. This symmetry was demonstrated by the calculated zero side forces and by the approximately symmetric location of the separation lines on both sides of the model. Separation points were at larger angles from the front stagnation point in the cross-sectional planes near the nose portion than on the cylindrical portion of the model. On the cylindrical portion, most separation points were between 112.5 and 135 degrees.

The shear layers separated from the model and formed concentrated vortices on the right side at X/D = 2.4 and X/D = 7.0, and on the left side at X/D = 4.8. These locations were obtained with the procedures discussed in the previous section. However, as shown in the Schlieren photograph (Figure 21), the vortices traveled near the missile body for a short distance before they became aligned with the free stream. This phenomenon is more pronounced near the model nose. Therefore, the true vortex breakaway points probably lie ahead of those indicated in the AEDC report. By comparing the vortex breakaway points with the axial pressure distribution curves, it was found that these points were located in the region where adverse pressure gradients occurred, as shown in Figure 30 and Figure 31. This means that the vortex breakaway points might be the separation points in the axial direction.

The side force distribution curve indicated two relative extremes. It can be seen that this side force distribution would result in a large

yawing moment on the model. A comparison of the side force extremes with either the separation lines or the vortices' breakaway points showed no significant correlation.

For the second data set ($M = 0.4, \alpha = 40$ degrees, $\phi = 45$ degrees), the separation points around the two sides of the model for each cross-sectional plane differed by approximately 90 degrees. On the left side of the model separation points were between 45 degrees and 90 degrees, whereas on the right side, between 135 degrees and 180 degrees, as shown in Figures 28 and 29. The same situation as the first set of data was obtained in studying the vortex breakaway locations with respect to axial pressure distribution, as shown in Figures 32 and 33. Other results such as side force distribution and vortex breakaway locations showed no correlation. The drastic change in separation locations between the two sets of data raised some doubts on the validity and accuracy of the data selected for this analysis. In view of the limited data analyzed in this study and the apparent discrepancies, it is essential to obtain some three-dimensional data, which contains more measurements in the separation zone.

6.0 CONCLUSIONS

In this research, the following conclusions were obtained:

1. Stratford's separation criterion is satisfactory for turbulent boundary layer separation calculations.
2. Stratford's separation criterion can be applied to three-dimensional problems, if the flow field can be divided into two independent flow directions.
3. Separation locations can be determined on slender bodies at high angles of attack by treating the cross-flow as being uncoupled from the axial flow.
4. Vortex breakaway locations may be predicted by applying Stratford's separation criterion to the pressure distribution along the previously calculated cross-flow separation line.
5. No apparent correlation between side force and separation lines/vortex breakaway points was found.
6. More detailed experimental data is needed for this complex three-dimensional problem. These data should include detailed surface pressure distributions, velocity profiles, separation locations, determination of surface streamlines, and wake flow characteristics.

REFERENCES

1. Przirembel, C.E.G., "Aerodynamics of Slender Bodies at Angles of Attack - A Critical Review", AFFDL-TM-76-92-FXG, Wright-Patterson Air Force Base, Ohio, Air Force Flight Dynamics Laboratory, August 1976.

2. Fleeman, E.L. and Nelson, R.C., "Aerodynamic Forces and Moments on A Slender Body with a Jet Plume for Angles of Attack Up to 180 Degrees", AIAA Paper No. 74-110, AIAA 12th Aerospace Sciences Meeting, Washington, D.C., February 1974.

3. Coe, P.L., Jr., Chambers, J.R., and Letko, W., "Asymmetric Lateral-Directional Characteristics of Pointed Bodies of Revolution at High Angles of Attack", NASA TN D-7095, November, 1972.

4. Deffenbaugh, F.D., and Koerner, W.G., "Asymmetric Wake Development and Associated Side Force on Missiles at High Angles of Attack", J. of Spacecraft, Vol. 14, March 1977, pp. 155-162.

5. Cebeci, T., Mosinskis, G.J., and Smith, A.M.O., "Calculation of Viscous Drag and Turbulent Boundary Layer Separation on Two-Dimensional and Axisymmetric Bodies in Incompressible Flows", Report MDC J0973-01, Douglas Aircraft Company, 1970.

6. Truckenbrodt, E., "A Method of Quadrature for Calculation of the Laminar and Turbulent Boundary Layer in Case of Plane and Rotationally Symmetric Flow", NACA TM1379, 1955.

7. Head, M.R., "Entrainment in the Turbulent Boundary Layer", Report R. and M. 3152, Aeronautical Research Council, England, 1960.

8. Cebeci, T., Mosinskis, G.J., and Smith, A.M.O., "Calculation of Separation Points in Incompressible Turbulent Flows", J. of Aircraft, Vol. 9, No. 9, September, 1972, pp. 618-624.

9. Stratford, B.S., "The Prediction of Separation of the Turbulent Boundary Layer", J. of Fluid Mechanics, Vol. 5, 1959, pp. 1-16.

10. Townsend, A.A., "The Behavior of a Turbulent Boundary Layer Near Separation", J. of Fluid Mechanics, Vol. 12, 1962, pp. 536-554.

11. Sandborn, V.A., and Liu, C.Y., "On Turbulent Boundary Layer Separation", J. of Fluid Mechanics, Vol. 23, 1968, pp. 293-304.

12. Schubauer, G.B., and Klebanoff, P.S., "Investigation of Separation of the Turbulent Boundary Layer", NACA TN 2133, 1950.

13. Schubauer, G.B., "Air Flow in the Boundary Layer of an Elliptic Cylinder", NACA TR 652, 1939.

14. Roshko, A., "Experiments on the Flow Past a Circular Cylinder at High Reynolds Number", J. of Fluid Mechanics, Vol. 10, 1961, pp. 345-356.

15. Yi, C.H., "Incompressible Turbulent Separation from an Axisymmetric Curved Afterbody", Ph.D. Thesis, Rutgers University, June 1972.

16. Achenbach, E., "Distribution of Local Pressure and Skin Friction Around a Cylinder in Cross-Flow up to Re = 5 x 10^6", J. of Fluid Mechanics, Vol. 34, Part 4, 1968, pp. 625-639.

17. Turelli, R.R., "An Experimental Investigation of Steady Asymmetric Vortex Shedding from a Slender Body of Revolution at High Angles of Attack", AFFDL GAE/AE/77D-7, 1977.

SECURITY CLASSIFICATION OF THIS PAGE (When Data Entered)

REPORT DOCUMENTATION PAGE

READ INSTRUCTIONS BEFORE COMPLETING FORM

1. REPORT NUMBER: AFOSR-TR-79-0022	2. GOVT ACCESSION NO.
3. RECIPIENT'S CATALOG NUMBER	
4. TITLE (and Subtitle): BOUNDARY LAYER SEPARATION FROM A SLENDER BODY AT HIGH ANGLES OF ATTACK	5. TYPE OF REPORT & PERIOD COVERED: FINAL, March 1977 — June 1978
6. PERFORMING ORG. REPORT NUMBER: RU-TR-151-MIAE-F	
7. AUTHOR(s): C. E. G. PRIZIREMBEL, D. T. G. WEN	8. CONTRACT OR GRANT NUMBER(s): AFOSR-77-3300
9. PERFORMING ORGANIZATION NAME AND ADDRESS: RUTGERS UNIVERSITY, MECHANICAL, INDUSTRIAL, & AEROSPACE ENGINEERING DEPT, NEW BRUNSWICK, N J 08903	10. PROGRAM ELEMENT, PROJECT, TASK AREA & WORK UNIT NUMBERS: 2307D9, 61102F
11. CONTROLLING OFFICE NAME AND ADDRESS: AIR FORCE OFFICE OF SCIENTIFIC RESEARCH/NA, BLDG 410, BOLLING AIR FORCE BASE, D C 20332	12. REPORT DATE: Oct 78 13. NUMBER OF PAGES: 67
14. MONITORING AGENCY NAME & ADDRESS (if different from Controlling Office): 69 p.	15. SECURITY CLASS. (of this report): UNCLASSIFIED 15a. DECLASSIFICATION/DOWNGRADING SCHEDULE

16. DISTRIBUTION STATEMENT (of this Report)

Approved for public release; distribution unlimited.

17. DISTRIBUTION STATEMENT (of the abstract entered in Block 20, if different from Report)

18. SUPPLEMENTARY NOTES

19. KEY WORDS (Continue on reverse side if necessary and identify by block number)

HIGH ANGLE OF ATTACK
MISSILE AERODYNAMICS
FLOW SEPARATION

20. ABSTRACT (Continue on reverse side if necessary and identify by block number)

The boundary layer separation process associated with the flow field around a slender body of revolution at moderate to high angles of attack was investigated. Based on extensive comparison with existing two-dimensional, turbulent separation data, flow separation criteria by Stratford, and Sandborn and Liu were selected for the slender body calculations. The two primary axial separation lines were obtained by applying the separation criteria to the measured surface pressure distributions in numerous crossflow planes. The location of the origin of the asymmetric vortices were predicted by applying Stratford's separation criterion

DD FORM 1 JAN 73 1473

400 607

UNCLASSIFIED

SECURITY CLASSIFICATION OF THIS PAGE (When Data Entered)

to the pressure distribution along the previously calculated axial separation line. Good agreement between the analytical and experimental points was obtained. Correlation between the side force maxima or minima and the location of the origin of the axisymmetric vortices was inconclusive. The need for more detailed experimental data is discussed.